Dipartimento
di Fisica
e Astronomia
Galileo Galilei

**Università degli Studi di Padova**

DIPARTIMENTO DI FISICA E ASTRONOMIA
DIPARTIMENTO DI INGEGNERIA INDUSTRIALE
Corso di Laurea in Fisica

# Theoretical analysis and experimental evaluation of the effect of landing shapes on snowboard jump dynamics

Candidato:
**Tomelleri Linda**
**Matricola 1005401**

Relatore:
**Prof. Petrone Nicola**

Correlatore:
**Prof. Gasparotto Andrea**

**Anno Accademico 2014–2015**

*Dedicato a*
*chi mi è stato accanto*
*e chi ho incontrato durante questo percorso*
*perché, in un modo o nell'altro,*
*hanno tutti contribuito*
*a realizzarlo e renderlo speciale.*

Thanks to
Prof. Nicola Petrone and Giuseppe Marcolin,
Jeffrey Campbell and all the ISEA Winter School tutors and participants,
Matteo Cognolato, Omar Quagliotto and all my laboratory's mates,
my family and Luna, Alessio, Eleonora, Laura, Valentina and Matteo,
Prof. Piero Martin for encouraging me to develop this project.

A special thanks to
Prof. Mont Hubbard, his willingness and fundamental contribution.

# Contents

# 1 Introduction

One of the most popular activities regarding the increasingly popular sport of snowboarding and free-style skiing is 'catching air': the rider by launching himself from a jump feature, which is usually either natural or man-made, performs an air manoeuvre, and lands safely. Therefore, almost all ski areas today have been provided with terrain parks, in order to satisfy the users' desires. However, snowboarders and skiers' injuries, including permanently debilitating traumatic brain and severe spinal cord traumas, have increased dramatically over the last two decades. Moreover, these injuries largely occur when skiers and snowboarders land from jumps and other aerial features. This primarily occurs since most jump landing surfaces are not designed according to scientific procedures, on the contrary they are built by the terrain park personnel, who does not employ a scientific and systematic method of design. Although these jumps are usually tested before being opened to the skiing public, they frequently cause large impulses at the moment of the landing impact that are severe enough to cause the injuries above-mentioned. This unwillingness of ski resorts to embrace an engineering design approach can be apparently ascribable to their risk management strategy. Furthermore, the skiing industry argues that the design process is currently too susceptible to changes under snow conditions, including snow melting and accumulation, and other factors (e.g. variations in jumper aerodynamic drag, jumper 'pop') which cannot be controlled both by a scientific design, in maintenance, or during the actual use. Specifically, the NSAA[1] asserts that, due to the rider and snow variability, terrain park jump 'standards are impossible'. Despite these uncontrollable factors, it should be mentioned that a specific standard design can be substantially insensitive to them. In spite of this reluctance of the skiing industry to employ a specific design, matters appear to be changing. Committee F-27 on Snow Skiing of ASTM[2] is in the process of voting to bring recreational winter terrain park jumps within its purview and has created a Terrain Park Task Group. It therefore appears probable that engineering design approaches will soon be applied to winter terrain park jumps.

# 2 Research project

The aim of this work was to verify a novel and safer jump's profile. First and foremost, a theoretical model has been analysed both for the design and the human motion. In the second instance, the experimental evaluation of the theory has been developed. The project has been fulfilled by adopting both a point-mass and a two-point-mass model. As a first step, an attempt to easily describe the motion has been performed in the laboratory. Both the models have been analysed during these test sessions. Afterwards, the two-point-mass model has been chosen for the in field experiment. The evidences which emerge from the laboratory's results have been employed for the in field data analysis. Simultaneously, a geometrical validation of both the tabletop and the safer jump's profile with their own safety's function has been accomplished. Although this work does not concerns the whole innovative terrain park's design, the part examined seems to satisfy the expectations. This fact should encourage to further in improving the research.

[1] National Ski Areas Association
[2] American Society for Testing and Materials

# 3 Design criteria

## 3.1 Field conventions

First of all it is due to assign an univocal label to each relevant terrain park zone, starting from the standard tabletop jump (Figure 1).

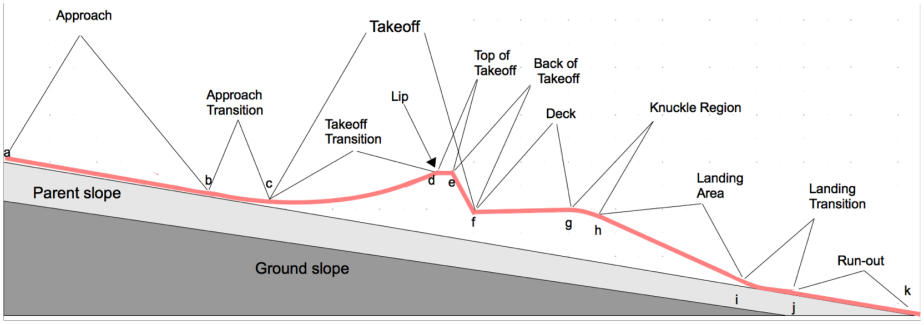


Figure 1: Tabletop jump

1. *Approach*: the downhill sloping surface leading into the Approach Transition
2. *Approach Transition*: the curved surface connecting the Approach to the horizontal which marks the start of the Takeoff
3. *Takeoff*: the part of the jump whose surface connects the (horizontal) end of the Approach Transition to the end of the back of the takeoff
   (a) *Takeoff Transition*: the first part of the Takeoff whose surface begins at the horizontal and ends at the Lip
   (b) *Lip*: the end of the takeoff surface where the surface angle departs from the takeoff angle
   (c) *Top of Takeoff*: the generally horizontal section after the lip and before the back of the takeoff
   (d) *Back of Takeoff*: the surface connecting the end of the top of the takeoff to the start of the deck of the jump (or landing area if there is no deck)
4. *Deck*: the surface between the back of the takeoff and the start of the knuckle
5. *Knuckle Region*: the transition between the deck and the landing surface
6. *Landing area*: the surface between the knuckle region and the landing transition
7. *Landing Transition*: the surface between the landing area and the start of the run-out
8. *Run out*: the parent slope that follows the end of the landing transition

## 3.2 Jump devise

The released energy constitutes the main reason for injuries occurred in terrain parks during the landing impact. Thus, engineering parameters correlated to this factor should be kept under accurate control. Firs of all, landing phenomena should be simplified (i.e. the neglecting of all the dissipative forces, acceptable for velocities roughly less than $18\,\frac{m}{s}$, and the three-dimensionality of the human body) in order to understand which physical quantities are fundamental. The well-known concept of the fall height in a free fall lies at the base of these calculation, and is obtained from the conservation of energy:

$$h = \frac{v^2}{2g}$$

In the light of these approximations, the snowboard jump may be regarded as a parabolic motion. As a consequence, the concept of fall height should be modified in an equivalent fall height. (Figure 2):

$$EFH = \frac{v_\perp^2}{2g} = \frac{(v_J \sin\alpha_J)^2}{2g} = \frac{v_J^2 \sin^2(\theta_J - \theta_L)}{2g} \tag{1}$$

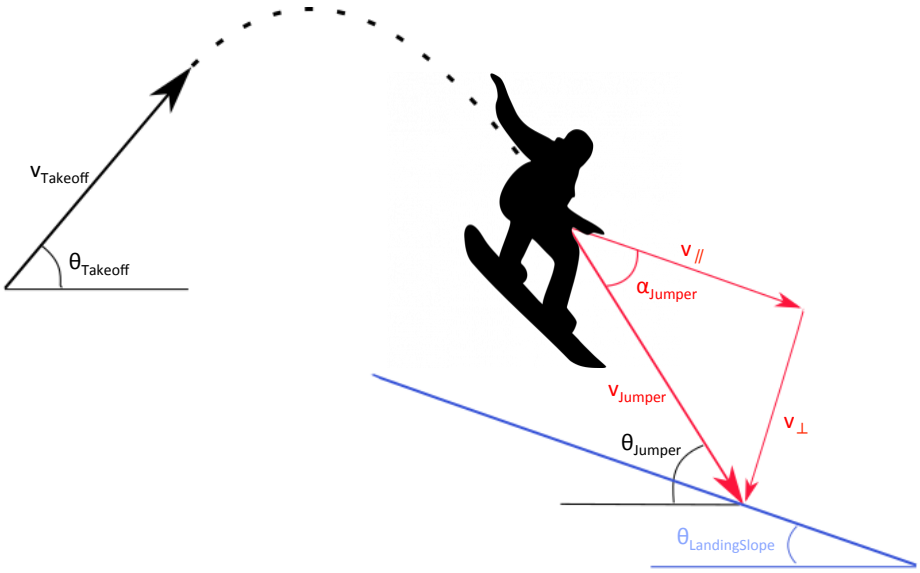


Figure 2: Equivalent fall height

This basic notion reveals that the landing impact can be easily controlled by managing the $EFH$. This height is strictly connected to the landing's slope with respect to the jumper's landing spot. By modelling the jumper as a point mass, it is possible to describe his motion using the projectile equation

$$x = v_{Tx}t \tag{2}$$

$$y = v_{Ty}t - \frac{1}{2}gt^2 \tag{3}$$

$$v_x \;=\; v_{Tx} \;=\; v_T \cos\theta_T \tag{4}$$

$$v_y \;=\; v_T \sin\theta_T - gt \tag{5}$$

by eliminating time from (2) and (3), the parabolic vertical position $y$ of the jumper flight path can only be written as the variable $x$ and the parameters $v_0$ and $\theta_T$

$$y \;=\; x\tan\theta_T - \frac{gx^2}{2(v_T\cos\theta_T)^2} \tag{6}$$

finally, by solving (6) for $v_T$ it can be found an expression for the jumper's initial velocity needed in order to reach a certain point $(x, y)$

$$v_T \;=\; \sqrt{\frac{gx^2}{2(x\tan\theta_T - y)cos^2\theta_T}} \tag{7}$$

The total velocity can be rewritten, using (4) and (5), as

$$v \;=\; \sqrt{v_x^2 + v_y^2} \;=\; \sqrt{(v_T\cos\theta_T)^2 + (v_T\sin\theta_T - gt)^2} \tag{8}$$

and again by eliminating $t$ from (8), the following expression emerges. It indicates the jumper's velocity at an arbitrary $(x, y)$ position in flight

$$v \;=\; \sqrt{(v_T\cos\theta_T)^2 + \left(v_T\sin\theta_T - \frac{gx}{v_T\cos\theta_T}\right)^2} \tag{9}$$

Once the expression of $v_T$ is stated with respect to $x$, $y$ and $\theta_T$, it is possible to substitute (7) in (9) in order to describe $v$ at any $(x, y)$ coordinates along the flight path knowing only the takeoff angle $\theta_T$

$$v \;=\; \sqrt{\frac{gx^2}{2(x\tan\theta_T - y)\cos^2\theta_T} - 2gy} \tag{10}$$

The last step needed to obtain a useful formula for the $equivalent\ fall\ height$ is to describe the jumper and the landing angles with respect to $x$, $y$ and $\theta_T$, as already done for the velocity

$$\theta_L \;=\; \arctan\left(\frac{dy_L}{dx}\right) \;=\; \arctan y_L'(x) \tag{11}$$

$$\theta_J \;=\; \arctan\left(\frac{dy}{dx}\right) \;=\; \arctan\left(\frac{v_y}{v_x}\right) \;=\; \arctan\left(\frac{2y}{x} - \tan\theta_T\right) \tag{12}$$

The $equivalent\ fall\ height$ can now be rewritten by substituting the expressions (10) with $v$, (11) with $\theta_T$ and (12) with $\theta_J$, obtaining

$$\begin{aligned} EFH \;=\; &\left[\frac{x^2}{4(x\tan\theta_T - y_L(x))\cos^2\theta_T} - y_L(x)\right]\cdot \\ &\cdot\sin^2\left[\arctan\left(\frac{2y_L(x)}{x} - \tan\theta_T\right) - \arctan y_L'(x)\right] \end{aligned} \tag{13}$$

which expresses the $EFH$ of any jump landing scenario as a function of the variables $x$, $y$ on the flight path at landing and the jump design parameters $\theta_T$ and $\theta_L$ or, more precisely, the $profile\ landing\ derivative$. It is important to emphasize that (13) is a completely general equation and can be thus applied to every landing on any jump landing surface at any landing point $(x, y_L)$, with a landing surface slope $\theta_L$ and from a takeoff angle $\theta_T$ (Figure 3). Although $EFH$ represents only one factor, for a given takeoff angle any landing surface shape $y_L(x)$ characterises the relative safety of the jump through the function $EFH(x)$. There are some possible applications of (13): it can be used to test the adequacy of a proposed landing surface shape $y_L(x)$, or as an indicator of the safety of an already fabricated shape. In each case, the $EFH$ should be relatively small everywhere if it aims at having a jump with the least possible injuries (at every possible landing positions $x$). The USTPC[3] established a maximum acceptable $EFH$ of $1.5\,m$, which correspond to the ability of a young athletic man to absorb the vertical impulse and maintain control without compromising his knees. The landing area which meets this criterion shall be referred to as the 'soft-landing' region of the jump.

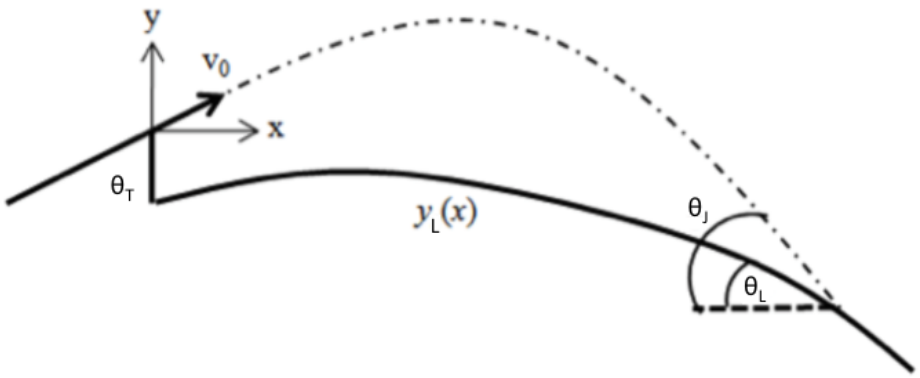


Figure 3: Generic jump profile

Notice that (13) depends on the jump profile and the landing point $(x, y_L)$, thus, by trying to invert it, the results is an ordinary differential equation, called the '$safe\ slope\ differential\ equation$'

$$y_L'(x) = \tan\left[\arctan\left(\frac{2y_L(x)}{x} - \tan\theta_T\right) + \right. \\ \left. + \arcsin\sqrt{\frac{EFH}{\frac{x^2}{4(x\tan\theta_T - y_L(x))\cos^2\theta_T} - y_L(x)}}\right] \tag{14}$$

Once chosen the initial parameters, $\theta_T$ and $v_T$, a constant $EFH = h$ and the boundary conditions $(x_L^{max}, y_L(x_L^{max}))$, (14) can be solved numerically in the range $(0, x_L^{max}]$ obtaining a jump profile which has an $EFH(x) = h,\ \forall x \in (0, x_L^{max}]$ (Figure 4). The freedom to choose the boundary condition means that there is a family composed by infinite $ODE$'s solutions. Therefore, among all the possible constraints, using the minimum amount of snow which is needed to match the

[3]US Terrain Park Council

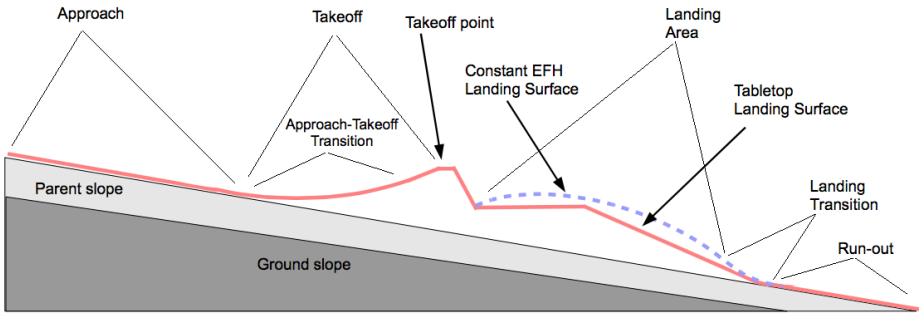


Figure 4: Constant EFH jump

parent slope, appears as the most reasonable strategy to determine which solution should be built. The $x_L^{max}$ is chosen by knowing the total available space for the entire structure, and calculating the maximum velocity which can be reached by the rider from the approach's starting point to the takeoff's lip. Indeed, by neglecting all the dissipative forces, any other velocity which can be achieved will be less than the velocity previously mentioned. This probably happens because the rider can start from a nearer point or he can be braked by the friction, while the jump's profile provides and equivalent fall height for any jump beneath the maximum one. Devices, GUIs and other tools are developing in order to aid the terrain park's personnels in the optimisation of the jump's building. On the other hand, most of the current jumps are tabletop (Figure 1), as already said. The whole process examined so far could be applied to the tabletop by using its own profile function (with respect to the system of reference chosen on the lip) which is

$$y_L = \begin{cases} y_t & x \leq x_t \\ (x - x_t)\tan\varphi + y_t & x > x_t \end{cases} \tag{15}$$

where $y_t$ is the deck's height, $(x_t, y_t)$ is the knuckle position and $\varphi$ is the landing region's angle. Consequently, it would be possible to calculate the $EFH$ in two separate regions: the deck and the landing, since a jump can be performed with an initial velocity which is less than the velocity needed to go beyond the deck and to land on the right landing region. For the deck's region (Figure 5), the total $EFH$ could be found by adding the constant $h_2$ to $h_1$, which is yielded by the the energy equation (18)

$$h_1 = \frac{v_{0y}^2}{2g} = \frac{v_0^2 \cos^2\theta_0}{2g} \tag{16}$$

then, by substituting the previously determined initial velocity (7), $h_1$ becomes

$$h_1 = \frac{x^2 \tan^2\theta_0}{4(x\tan\theta_0 + y_t)} \tag{17}$$

thereby, the total $EFH$ is

$$EFH = h_1 + h_2 = y_t + \frac{x^2 \tan^2\theta_0}{4(x\tan\theta_0 + y_t)} \tag{18}$$

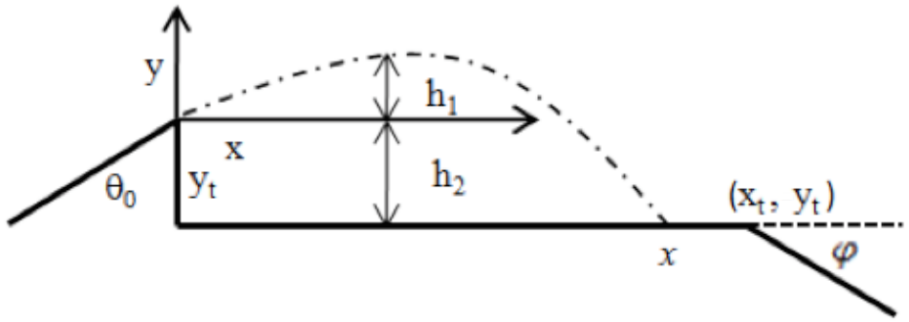


Figure 5: Tabletop deck

For the landing's region (Figure 6), the $EFH$ could be found substituting in (13) its own profile's function, which is (15) for $x > x_t$. This operation yields

$$EFH = \left[\frac{x^2}{4(x\tan\theta_0 - (y_t + (x - x_t)\tan\varphi))\cos^2\theta_0} - y_t - (x - x_t)\tan\varphi\right]\cdot \cdot \sin^2\left[\varphi - \arctan\left(\frac{2(y_t + (x - x_t)\tan\varphi)}{x} - \tan\theta_0\right)\right] \tag{19}$$

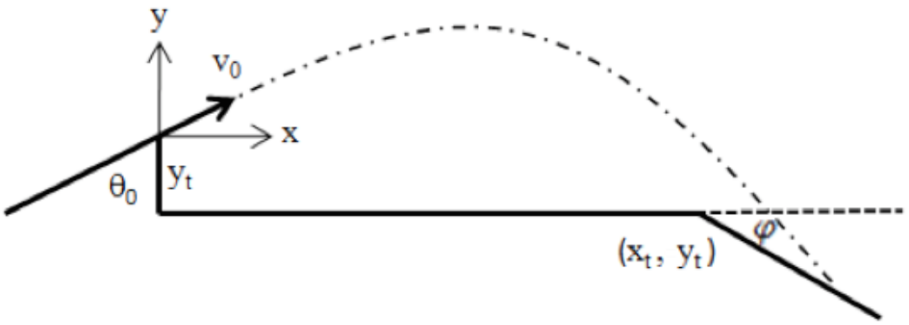


Figure 6: Tabletop landing

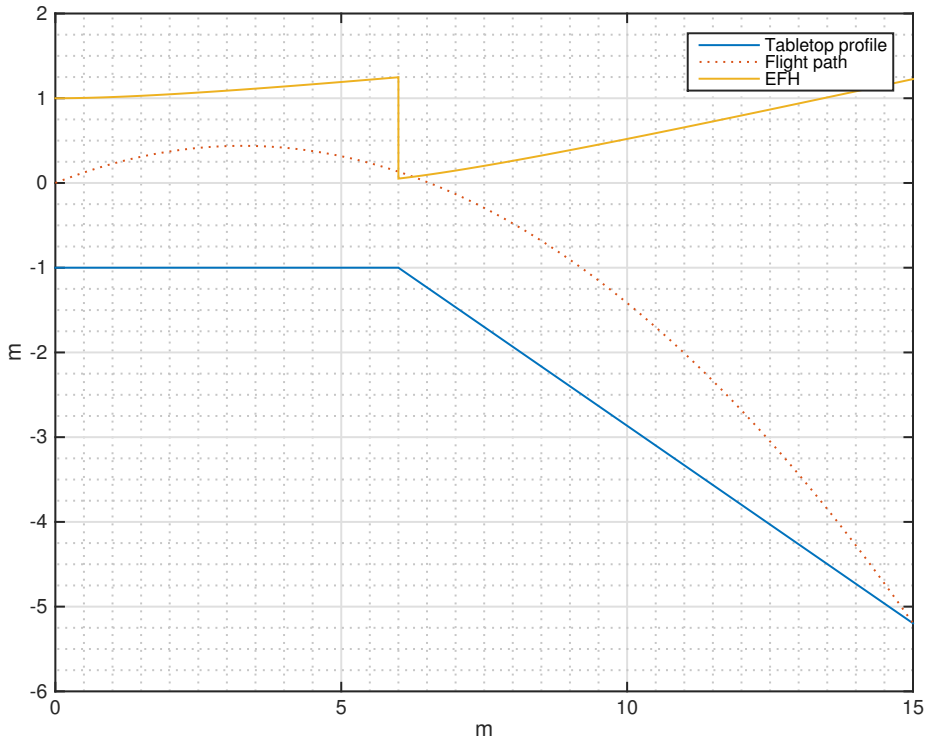


(a) Tabletop with parameters $\theta_T = 15°$, $v_T = 11.3\,ms^{-1}$, $x_L = 15\,m$, $H = 1\,m$, $D = 6\,m$

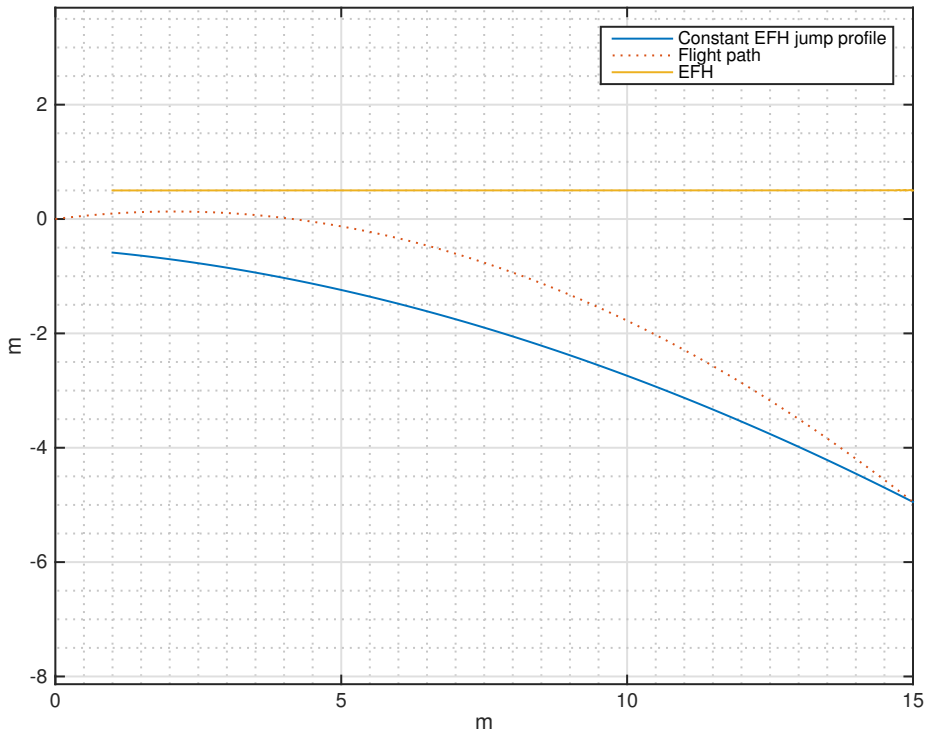


(b) Constant EFH jump designed with parameters and boundary conditions $\theta_T = 7.2°$, $v_T = 12.8\,ms^{-1}$, $x_L = 15\,m$, $EFH = 0.5\,m$

Figure 7: Tabletop and Constant EFH profiles with their own EFH functions

# 4 Laboratory one accelerometer jump analysis

## 4.1 Instrumentation and method

Due to the high complexity of the jumping movements, I attempted to describe in a clearer and easier way the athletic gestures. The instrumentation used during this experimental session was composed of one three-axial accelerometer, applied to the jumper's pelvis (Figure 8c), a motion capture system (Figure 9a), which was calibrated to record the positions of the markers applied to the key points (Figure 22b and Figure 8b) , one dynamometric platform (Figure 9b) and a videocamera. The aim of the work was to estimate how the previously adopted approximations, influence the evaluation of the $EFH$ by comparing three different heights obtained from three different methods. Firstly the height calculated from the elaboration of the accelerometer's signal, secondly from the dynamometric platform's one and thirdly from the motion capture's one. The strategy adopted was to perform $12$ jumps, which should end with a static flex position, in order to minimise dumping and vibrations. Since the comparison between two different results given by a force and by an acceleration was needed, the jumper was weighted before starting with the trials.

- Accelerometer:
  Somat SAPE-HLS-3010
  - $f = 5\,kHz$
  - measurement uncertainty $= \pm 2.5\%$
  - full range $= \pm 500\,g$
- Dynamometric Platform:
  Bertec FP4060
  - $f = 960\,Hz$
  - sensitivity $= \pm 2\,N$
- Motion Capture System:
  BTS CLASSIC
  - $f = 60\,Hz$
  - resolution $= 0.004\,m$

## 4.2 Data analysis

First of all, the jumper's mass has been evaluated by taking the mean and dividing by $g$ the measurements of a static weight on the dynamometric platform. After that, the dynamometric platform has been calibrated to measure $0\,N$ when the jumper is standing on it and every trial's signal has been divided by the mass, in order to be able to compare the two different sensors measurements. The system of reference which has been adopted was the ISB's[4] one, and thanks to the trunk's

[4] International Society of Biomechanics: y parallel to the longitudinal axis, x parallel to the sagittal axis (x can be chosen either parallel to the sagittal axis or to the transversal axis, depending on the kind of motion), z follows from the right-hand rule

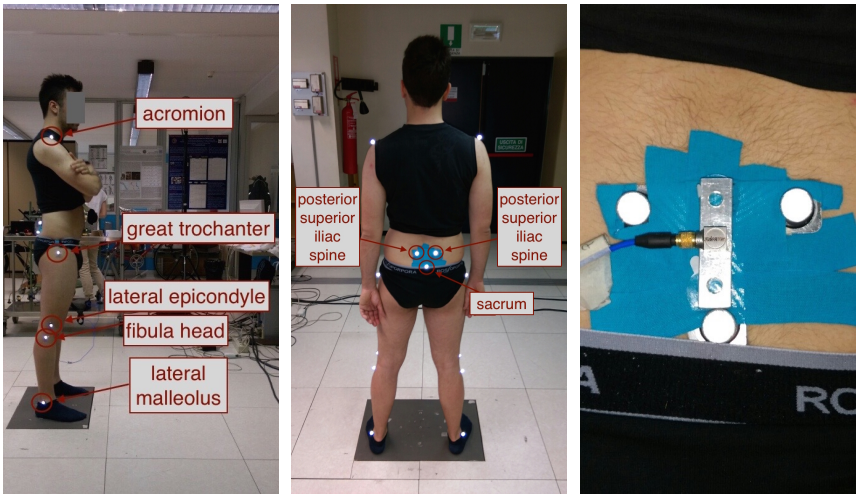


(a) Side view (b) Back view (c) Pelvis' detail

Figure 8: Markers and accelerometer

(a) IR cameras

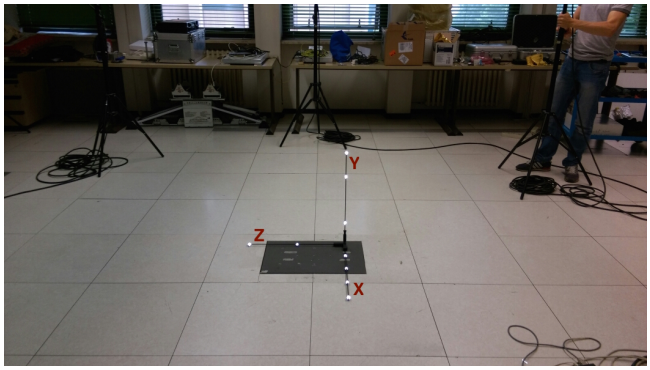


(b) Dynamometric Platform

Figure 9: Motion capture system

angle, which has been evaluated by the motion capture system, the longitudinal and the sagittal axis have been projected over the normal axis to the dynamometric platform's vertical one. These two signals have then be synchronised and this was possible thanks to three squats used as initial triggers before the jump. Thanks to the clarity of the platform's signal, which measures exactly $-g$ during the flight in contrast with the accelerometer which perceives any movement of the body, it is easer to find the impact's initial instant. This kind of measurement can be compared to a perfectly inelastic impact of a point-mass. Hence, all the energy should be dissipated. Therefore, $\Delta v$ can be evaluated by integrating both accelerations, which should be equal. Thus the strategy adopted was:

$$EFH_{acc} = \frac{v^2}{2g} = \frac{(v_f - v_i)^2}{2g} = \frac{(0 - v_i)^2}{2g} = \frac{\left(\int_{t_i}^{t_f} a_{acc}(t)dt\right)^2}{2g} \tag{20}$$

$$EFH_{plat} = \frac{v^2}{2g} = \frac{(v_f - v_i)^2}{2g} = \frac{(v_f - 0)^2}{2g} = \frac{\left(\int_{t_i}^{t_f} a_{plat}(t)dt\right)^2}{2g} \tag{21}$$

The most difficult hurdle I met was to determine the exact end of the landing, due to the lack of a systematic method. Therefore, the final extreme for the integration has been chosen when the acceleration returns to zero, even though it is not taken for granted that it represents the end of the event. The movement, in fact, can be compared to a damped oscillation (Figure 10). Hence, a zero in the acceleration depicts a maximum or a minimum velocity's value. This strategy has been chosen because it easily determines the final instant and it provides a method of comparison between the use of one accelerometer rather than two, as it will be explained in the following chapter.

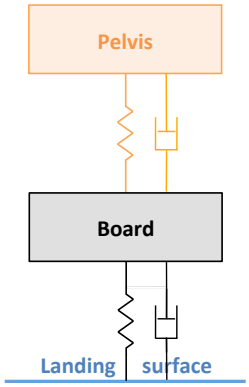


Figure 10: Body and board's spring model

The elaborated signal which has been used to evaluate the $EFH$ and the integration range's limits are shown by the graph in Figure 11, all the other trials are reported in the appendix. The chart in Figure 12 represents the comparison between the $EFH$s obtained from the different instrumentation for each trial.

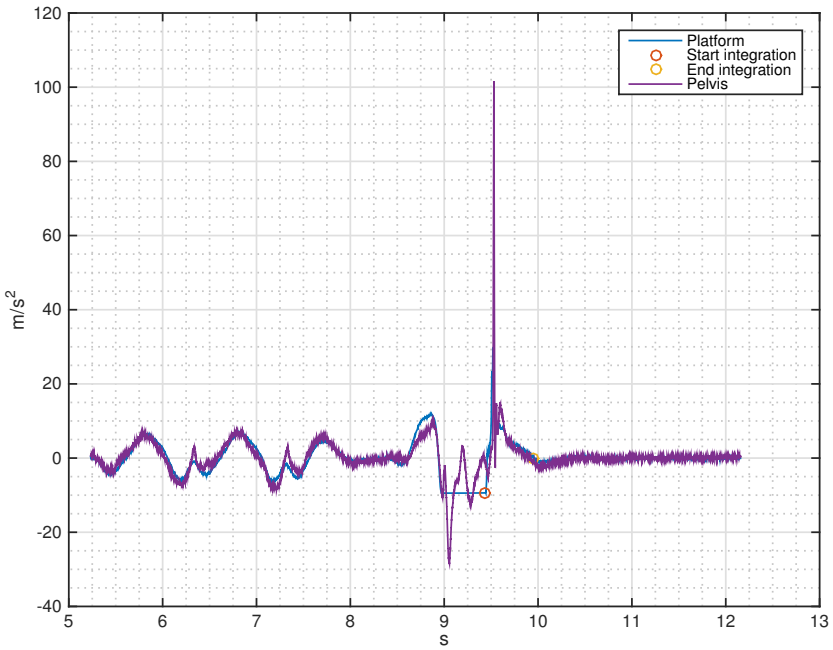


Figure 11: Acceleration

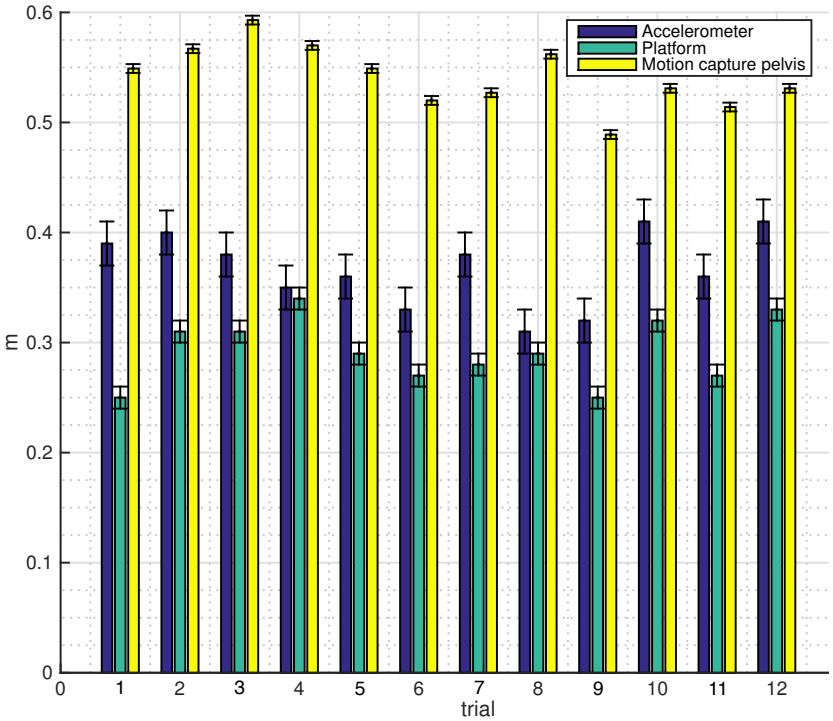


Figure 12: Results

# 5 Laboratory two accelerometers jump analysis

## 5.1 Instrumentation and method

Others 12 jumps were performed, moving as similar as possible, with a snowboard instead of the bare feet and a rubber mat on the dynamometric platform to prevent any possible structural damage (Figure 13a). Consequently, the jumper has been weighted once again. The instrumentation used is the same presented in the previous chapter with the addition of a second three-axial accelerometer applied to the centre of the snowboard (Figure 13a and Figure 13b). The purpose of this adjustment is to simulate the spring model mentioned/shown in figure (Figure 10).

- Board snd Pelvis' Accelerometers:
  Somat SAPE-HLS-3010
  - $f = 5kHz$
  - measurement uncertainty $= \pm 2.5\%$
  - full range $= \pm 500\, g$
- Dynamometric Platform:
  Bertec FP4060
  - $f = 960\, Hz$
  - sensitivity $= \pm 2\, N$
- Motion Capture System:
  BTS CLASSIC
  - $f = 60Hz$
  - resolution $= \pm 0.004\, m$

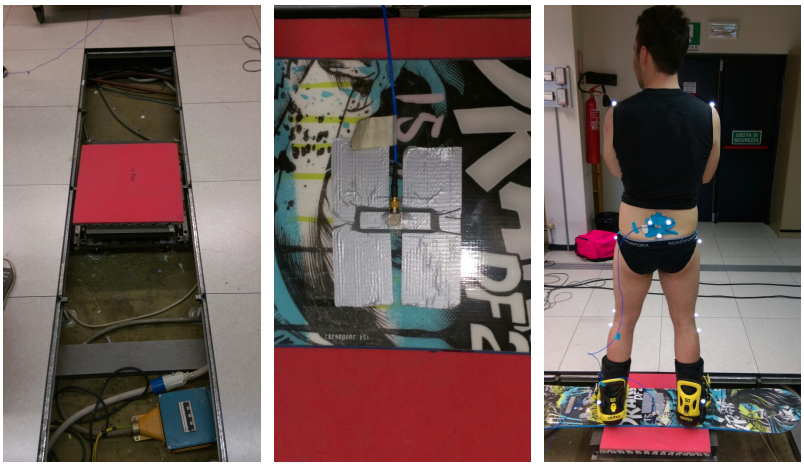

(a) Dynamometric platform with mat (b) Board's detail (c) Back view with snowboard

Figure 13: Accelerometers and dynamometric platform

## 5.2 Data analysis

The way to proceed in the data analysis has been identical to the one performed in the previous experimental section, with a different approach for what concerns the board's accelerometer and the choice of the final point for the integration. Considering the body and the board as a system of two masses and two springs (Figure 10), the landing could be simplified as it is represented in Figure 14. Figure 14a shows the jumper before the landing, while Figure 14b shows the moment after the landing when the board completely touches the ground with zero normal velocity. After that, the pelvis starts to be braked by the body's structures and, only when it arrives at its position's minimum, the velocity becomes the same of the board's one (Figure 14c). Moreover, the pelvis' movement is not yet completed while damping oscillations continue. When the pelvis starts to rise again, its normal velocity deviates from zero to the board's velocity when the normal pelvis' movement stops (Figure 14d).

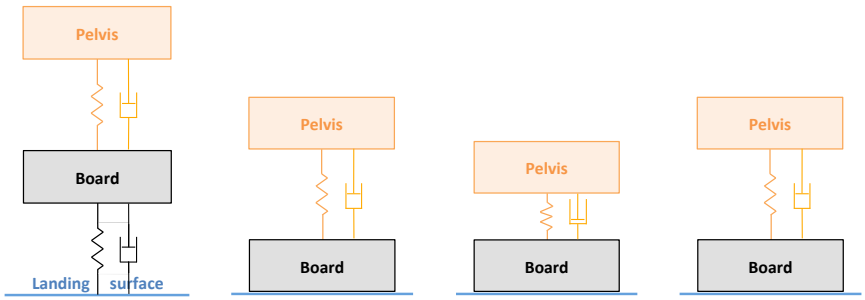


(a) Before landing (b) Board landing (c) Pelvis landing (d) Pelvis rebound

Figure 14: Spring model

The velocities are shown in Figure 16a, where it is possible to observe the crossing points: the first point, which has been chosen for the integration's extreme, represents Figure 14c while the second point represents Figure 14d. The elaborated signal which has been used to evaluate the $EFH$ and the integration range's limits are shown by the graph in Figure 16b, while all the other trials are reported in the appendix. The chart in Figure 17 represents for each trial the comparison between the $EFH$s obtained from the different instrumentation. Since the motion capture was not able to record the pelvis position during the $12^{th}$ trial, the pelvis' $EFH$ value has not been evaluated.

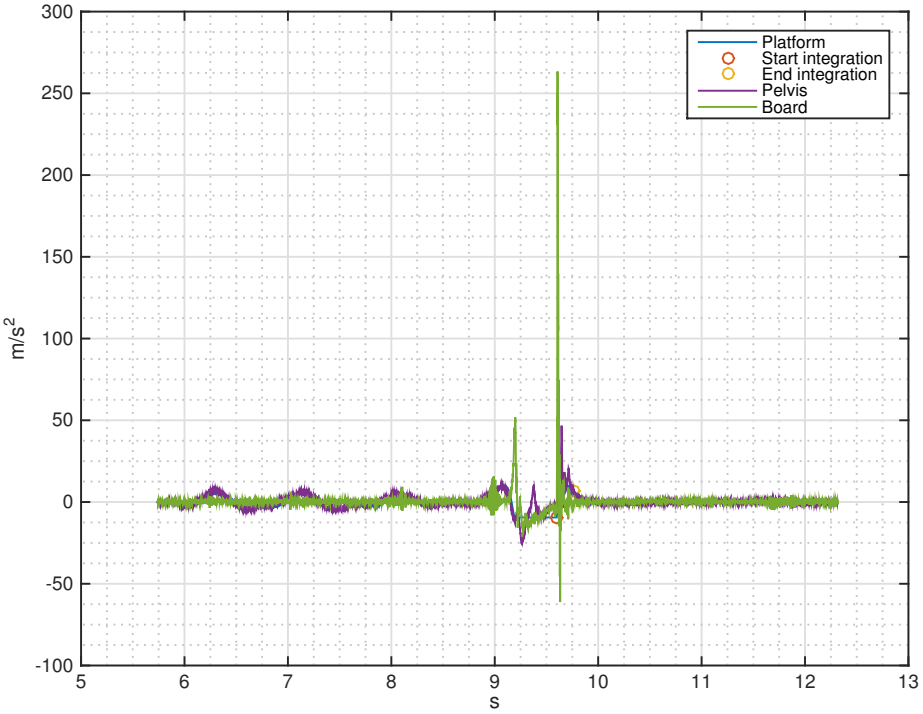


(a) Acceleration

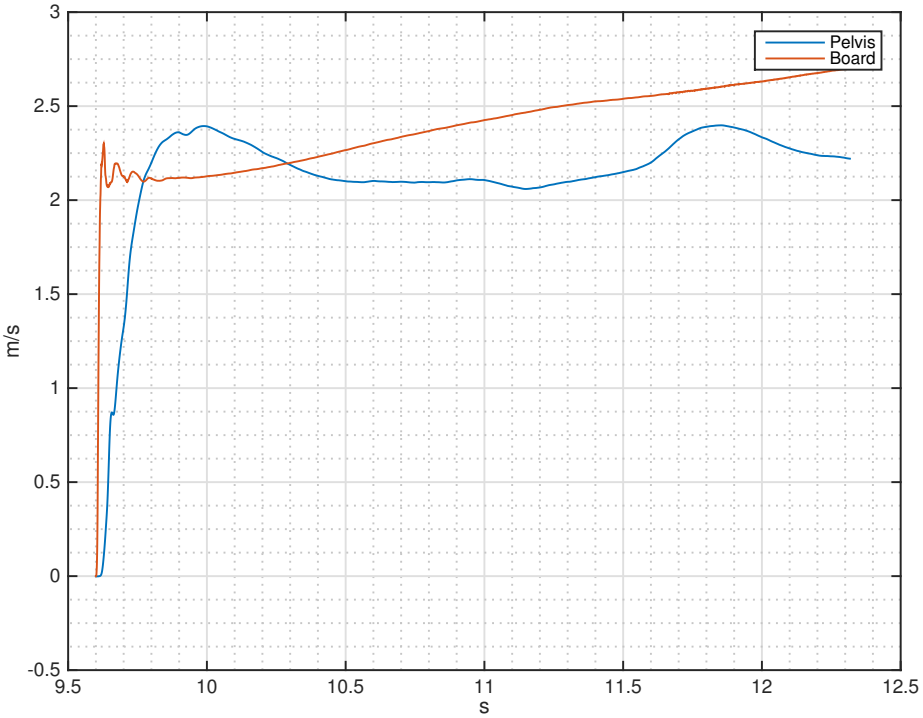


(b) Velocity

Figure 15: Jump signals

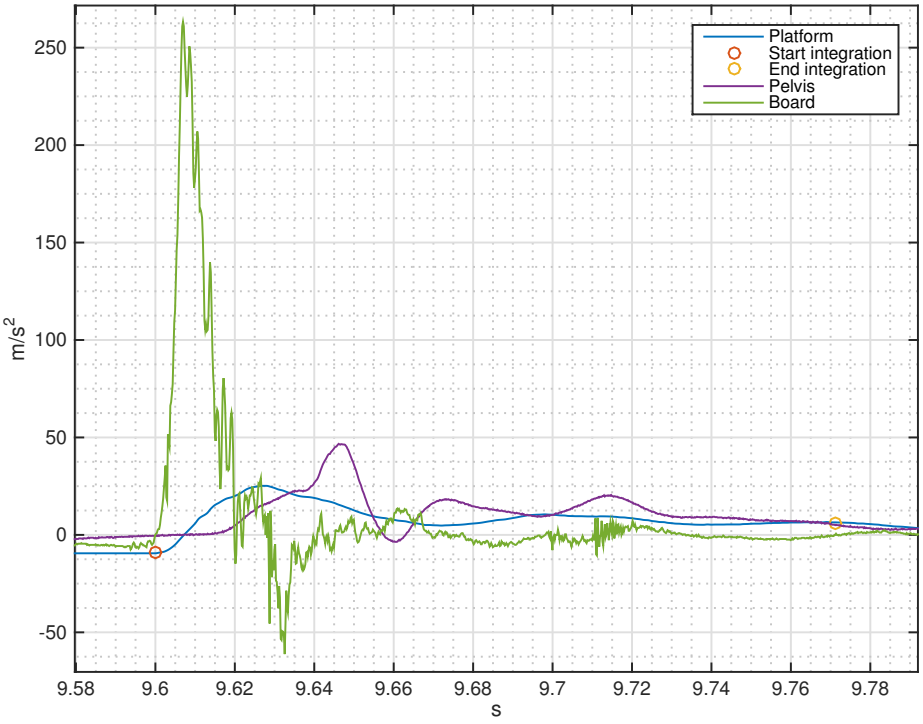


(a) Velocity

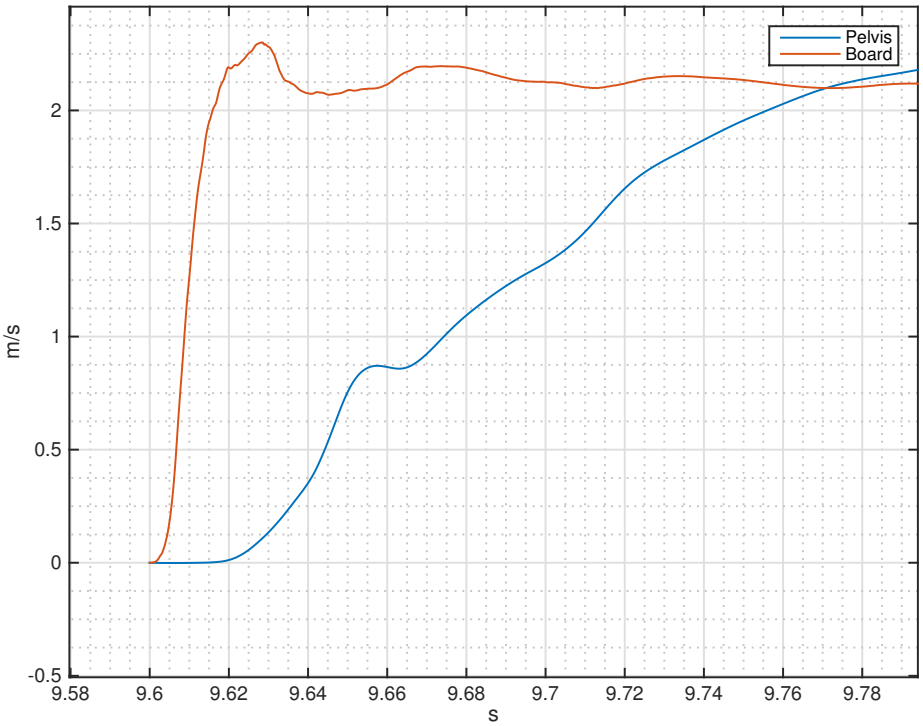


(b) Acceleration

Figure 16: Jump signals zoom

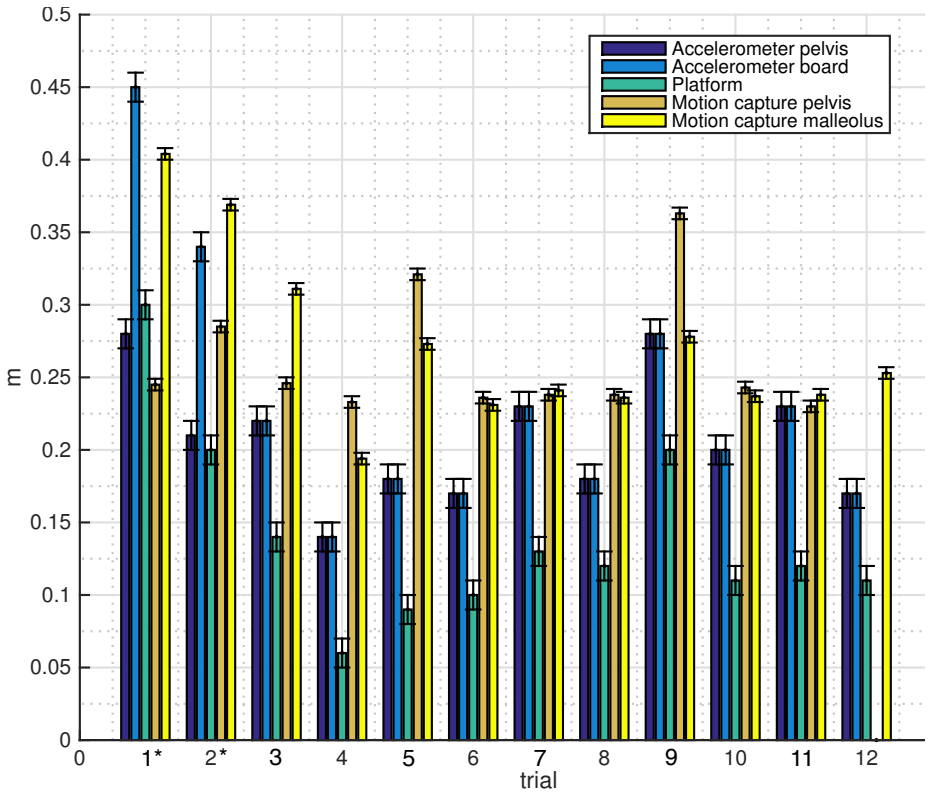


Figure 17: Results

The velocities evaluated for the trial $1^*$ and the trial $2^*$ do not cross (A.1.1 and A.1.2). This fact is probably due to the jumper's behaviour. Thanks to the videos, it is possible to notice that he flexes and then strongly extends his legs during the flight, just before landing. Therefore, the board is exposed to an acceleration which is considerably different from the pelvis' acceleration. As a consequence of this, only for these two trials, the integration's end has been chosen at the minimum distance between the pelvis and board's velocity.

# 6 In field EFH jump analysis

## 6.1 Jump design

### 6.1.1 Build and measurements

An attempt to build a $constant\ EFH$ jump was made during the 5th ISEA Winter School in Sports Engineering, which took place from 4th to 9th March 2015 in San Vito di Cadore (BL). The prospect was to model it with a constant $EFH$ of $0.5\,m$, reminding the USTP safety limit of $1.5\,m$, with the help of a snow groomer (Figure 18). The jump was then measured by using a measuring tape and a lever


Figure 18: Constant EFH jump profile

in order to obtain the curvilinear abscissa and its profile slope. The angle values ($\Delta\theta_L = \pm 0.1°$) were taken at every randomly selected length on the tape ($\Delta L = \pm 0.01\,m$), forward and backward with respect to the origin of the reference system chosen on the jump's lip.

### 6.1.2 EFH evaluation

After the measurements, an interpolation was processed in order to smoothly plot the jump profile and to calculate by (13) its relative $EFH(x)$ (Figure 19). Although an accurate design was processed before the jump's building, a not constant $EFH$ can be seen in Figure 19b. The cause may be ascribed to the hurdles which were encountered during the shaping, such as the adverse weather conditions and the groomer's lack of experience. Hence, the achieved real profile yields some irregularities, as its $EHF(x)$ (Figure 19b).

## 6.2 Instrumentation and method

During this session four accelerometers were used: one three-axial and three mono-axial (which were fastened onto a metal cube to simulate a three-axial one). They

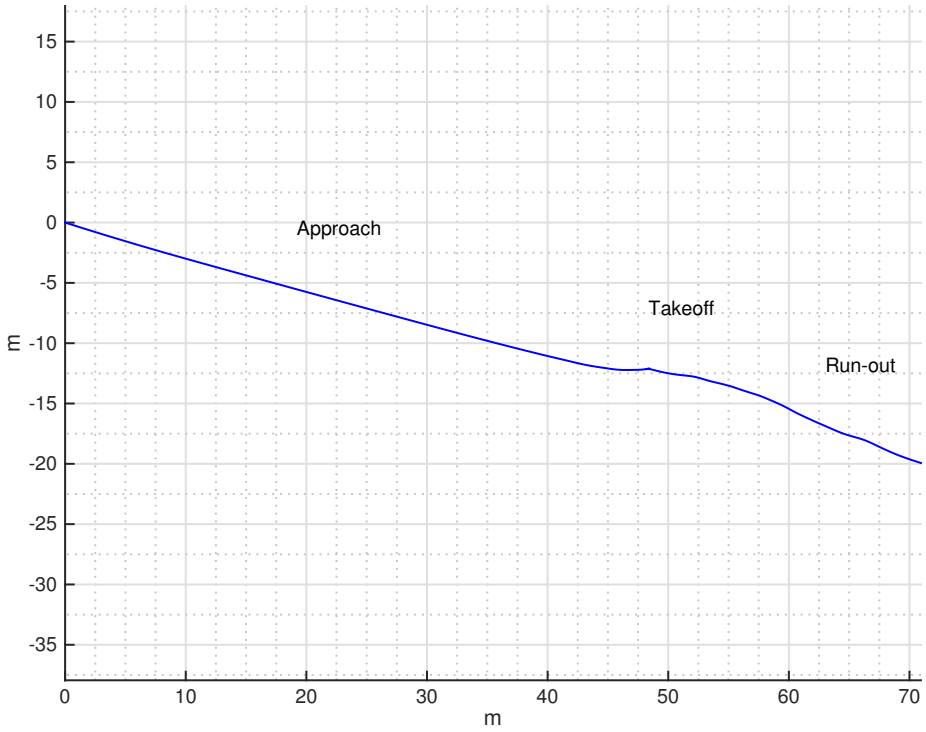


(a) Jump measured profile

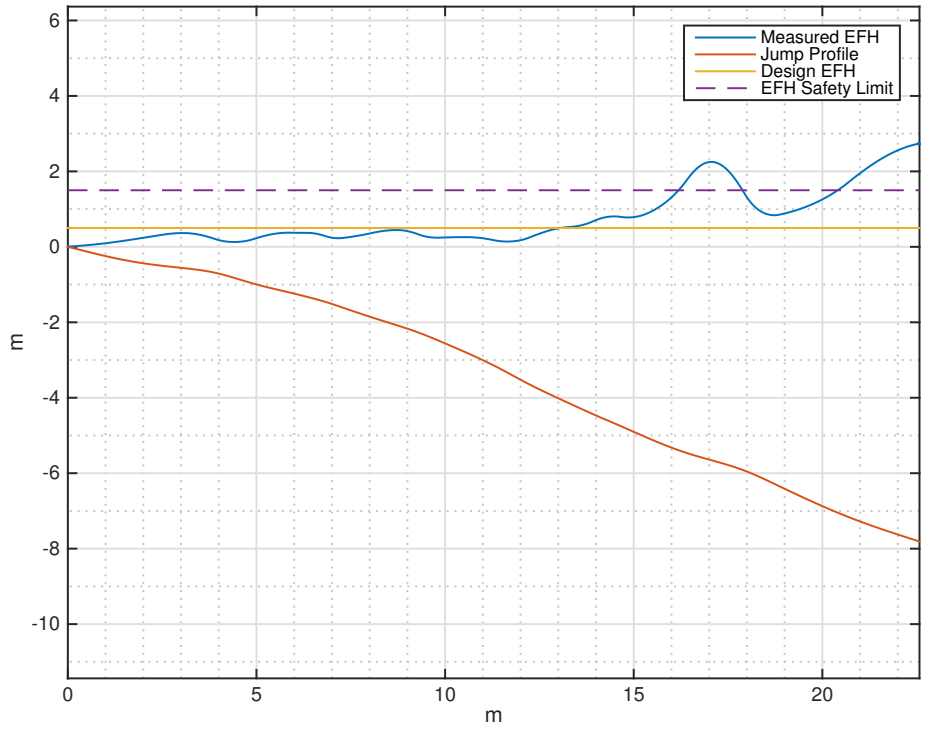


(b) Jump measured EFH

Figure 19: Jump profile

were applied to the jumper's pelvis (Figure 21a) and to the board (Figure 21b and 21c) with respect to their own reference system, as shown in Figure 20a. Furthermore,

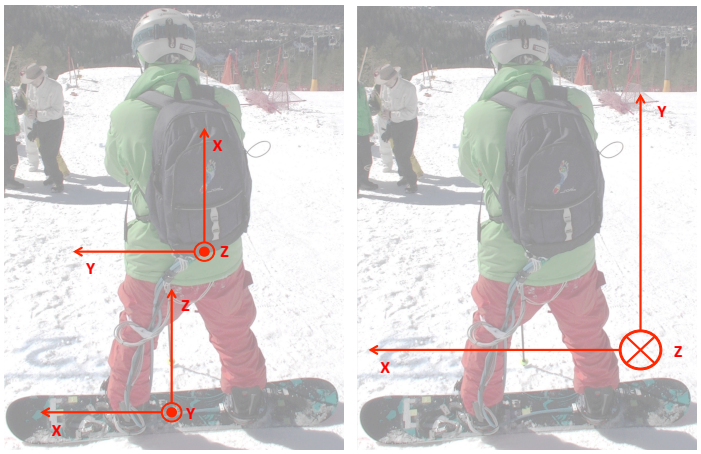


(a) Accelerometers (b) Modified ISB

Figure 20: Systems of reference

accordingly to a modified ISB[5] convention, both the systems of reference were changed as shown in Figure 20b. Then, the measuring session was subdivided in a total of eight jumps, divided into four different starting distances from the lip: two trials for each starting distance, beginning from $20\,m$ up to $50\,m$, $10\,m$ by $10\,m$, and backward. The jumper involved in the study was a snowboard instructor of 178 cm height and 82 kg mass using a 'regular' stance (left foot forward). Due to the theoretical approximations which were adopted, it was asked the rider to perform the jumps as stiff as possible in order to better represent the rigid body model. Furthermore, the approach and the transition, up to the takeoff, were faced as close as possible to a motion on an inclined plane, without considering the dissipative force (i.e. without braking or doing other movement which could change the nominal velocity at the takeoff and the flight path). Moreover, 'human eyes' were used to measure $x_L$, while a videocamera recorded each trial, with respect to the distance signed on the snow at every meter and poles every two meters.

- Pelvis' Accelerometer:
  DTS 6DX PRO
  - $f = 5kHz$
  - sensitivity $= 0.2\,mV/g$
  - full range $= \pm 2000\,g$
- Board's Accelerometer:
  Endevco 7264B-2000
  - $f = 5kHz$
  - sensitivity $= 0.20\,mV/g$
  - full range $= \pm 2000\,g$

[5] International Society of Biomechanics: x axis chosen along the transversal axis

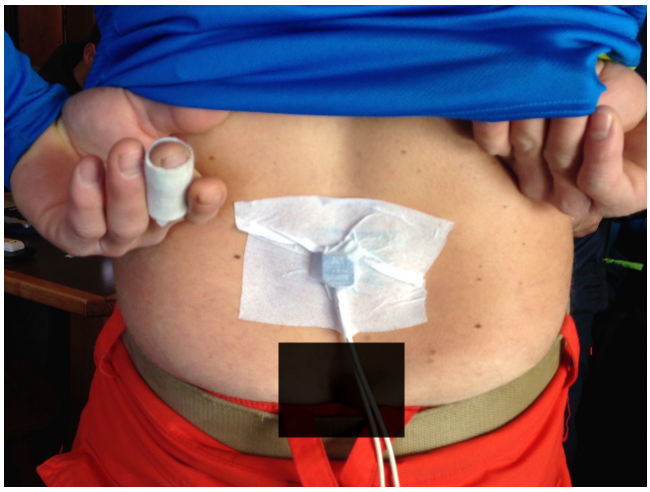

(a) Pelvis

(b) Board

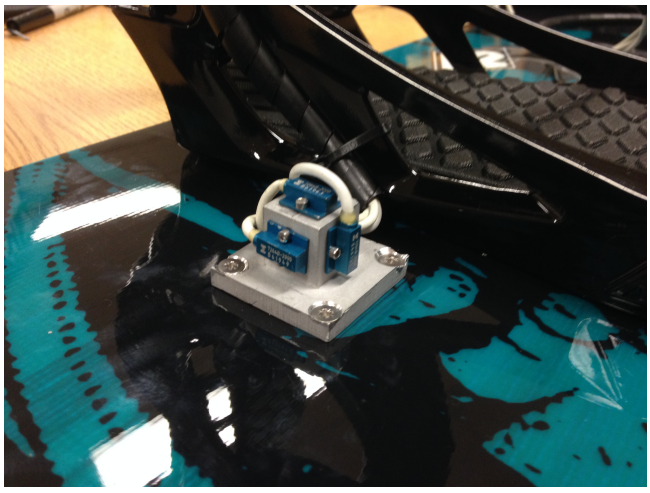

(c) Board detail

Figure 21: Accelerometers

## 6.3 Data analysis

The accelerometers were built to feel the static orientation, in contrast with all the previous trials, consequently every signal was influenced by the gravitational acceleration, i.e. during the flight the acceleration was $0\,g$ and during resting it was $1\,g$ (or any projection of $g$ over the axis). The effect of this choice could easily be seen from a not converging velocities graph. Moreover, the acceleration's integral had a bias which seems to be irrelevant in comparison to the accelerations' peaks. However, rather than conceptually wrong, this bias seems to considerably affects the small areas. Another difference between the tests performed in field and those performed in the laboratory, stood in the absence of the motion capture system in the former case. Thus, it was not possible to project the mobile jumper's axis on the surface's perpendicular at every time for all the runs. Due to the low temperature, the pelvis' accelerometer drifted and the data logger was not always able to maintain the calibration's zero (in this case to $1\,g$) presenting a different constant bias for each trial. Two different strategies have been adopted to avoid these unwillingness. First of all, a linear interpolation has been used to remove the thermal drift, since the jumper stayed for a short amount of time in the same position both at the beginning and at the end of each trial. Furthermore, as long as the constant bias is concerned, a calibration's hypothesis has been developed to set the signal at the right starting value. The initial standing position (Figure 22a), and the early riding position (Figure 22c), have been used as a reference by the following algorithm:

- standing
$$a_x = \tilde{a}_x - c_x = 0 \qquad \Rightarrow \qquad c_x = \tilde{a}_x \tag{22}$$
- early riding
$$a_z = \tilde{a}_z - c_z = 0 \qquad \Rightarrow \qquad c_z = \tilde{a}_z \tag{23}$$
- standing
$$|a| = \sqrt{a_y^2 + a_z^2} = g \qquad \Rightarrow \qquad c_y = a_y - \sqrt{g^2 - (\tilde{a}_z - c_z)^2} \tag{24}$$

where $c_x$, $c_y$ and $c_z$ are the bias, $a_x$, $a_y$ and $a_z$ are the unbiased accelerations and $\tilde{a}_x$, $\tilde{a}_y$ and $\tilde{a}_z$ are the biased accelerations for each axis. Unfortunately, during the fifth trial, the jumper fell and as a consequence, he probably damaged the wire connecting the z axis of the board's accelerometer to the data logger. Hence, another bias had been added to the signal, making it useless for this algorithm. The solution could be to use any other known parameter which describes the rider posture or any other relevant position. Since he used a snow racket to rest in a standing position, it could seem reasonable to assume that his body tend to follow the gravitational acceleration without many changes in the position, as shown in Figure 22b. Consequently, the board's z axis can be omitted because the y axis is the only one sensitive to $g$. By contrast, the pelvis is not well aligned to the body's longitudinal axis, as it has been shown in the lab tests. Thus, at any time, both the pelvis' z axis and y axis are susceptible to $g$. Furthermore, all the jumps had been performed by the rider as stiff as he could, for this reason the pelvis' angle $\alpha$ could be considered almost constant ($\approx 20°$) and it could be use both for the initial compensation and for the impact analysis. Once these considerations have been applied, the next step is to avoid the gravitational acceleration's influence. Since the time's interval of the impacts is less than $0.2\,s$ (because of the stiffer posture

than the tests performed in the laboratory), by using the videos it is possible to observe that the change in the jumper's position on the jump's profile during this $\Delta t$ does not cause considerable changes in the landing's angle $\theta_L$. As a consequence of this, the gravitational acceleration has been removed from the signal by calculating its projection.To do that the landing's angle was used, on the axis which is normal to the jump's profile, evaluated with $\alpha$ for the pelvis and using the y axis for the board.

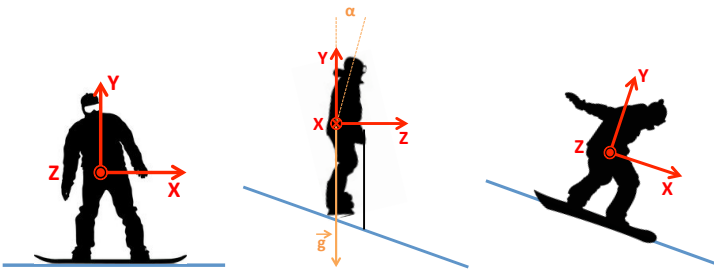


(a) Standing (b) Standing side view (c) Riding

Figure 22: Positions and system of references

The graph in Figure 23 shows the results obtained by following this method, in comparison with the $EFH$ function which has been estimated by the field's measurements.

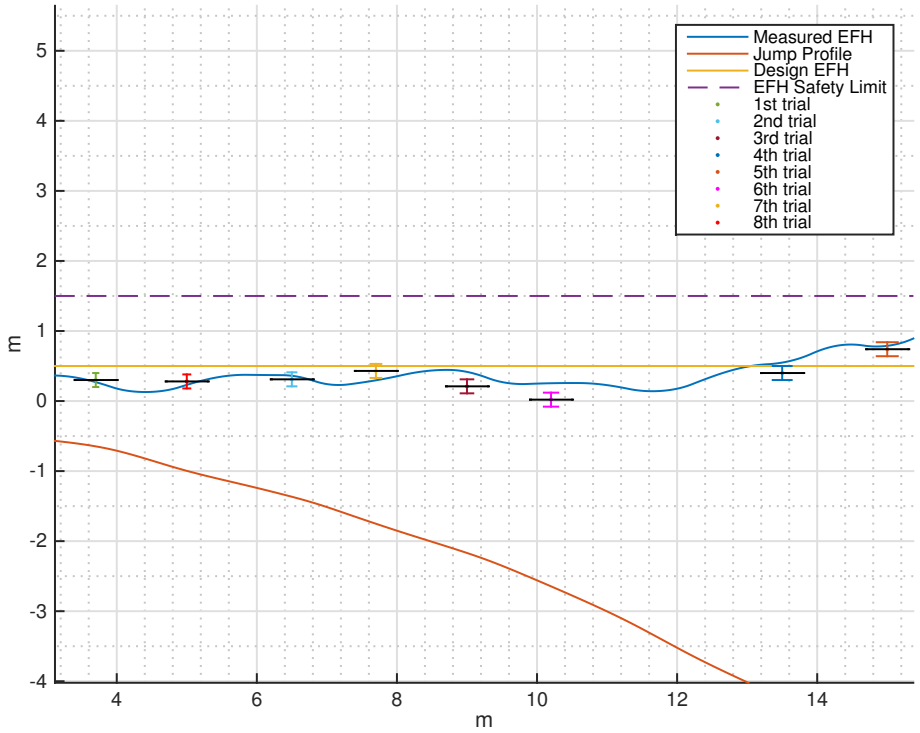


Figure 23: Results

# 7 Tabletop EFH evaluation

The second "in field" test session was executed in an already built snow park, Tognola Park in San Martino di Castrozza, where three sequential tabletop jumps were chosen to perform the trials. First of all, as done for the $constant\ EFH$ jump, the entire park profile was measured with a measuring tape and a lever, beginning from the approach and taking the angle's value at every randomly selected length until the takeoff transition start (Figure 1). Then, a value was taken for the lip, the top and the back of the takeoff. Finally, the angles of the deck and the landing were taken every meter up to $20\,m$. This procedure was repeated even for the second and the third jump, matching the landing end of the previous jump with the approach start of the following one. All the data were processed with an interpolation by a Matlab script which plots the entire park profile. This is a clear example of how the $EFH$ concept can be used as an indicator of the safety for an already fabricated shape, as explained in the second chapter. The measured tabletop $EFH$s are different from theoretical ones, as a consequence of the undefined design of jump, which provides lot of shape's imprecisions in comparison to the ideal profile. Nevertheless, by considering the approximations adopted to describe the tabletop profile (i.e. the perfectly horizontal deck, the angular knuckle, and the constant landing region's slope), the measured $EFH$ seems to be comparable to the theorised one. The $soft\text{-}landing$ region is properly situated within the knuckle and a certain distance on the landing (Figure 7a). What emerges from these three jumps is that the tabletop design provides two potentially dangerous zones. Therefore, an injury may occur both landing beneath and beyond the $soft\text{-}landing$ region. The more the knuckle is sharp-cornered, the more the $EFH$ function overlies the theoretical discontinuity between the deck and the landing. Even though the jump's end is clearly defined, the $constant\ EFH$ profile enlarges the $soft\text{-}landing$ region up to the back of the takeoff and extends its safety proprieties to any landing's position. This is reason of the huge potential lied behind this novel jump's shape.

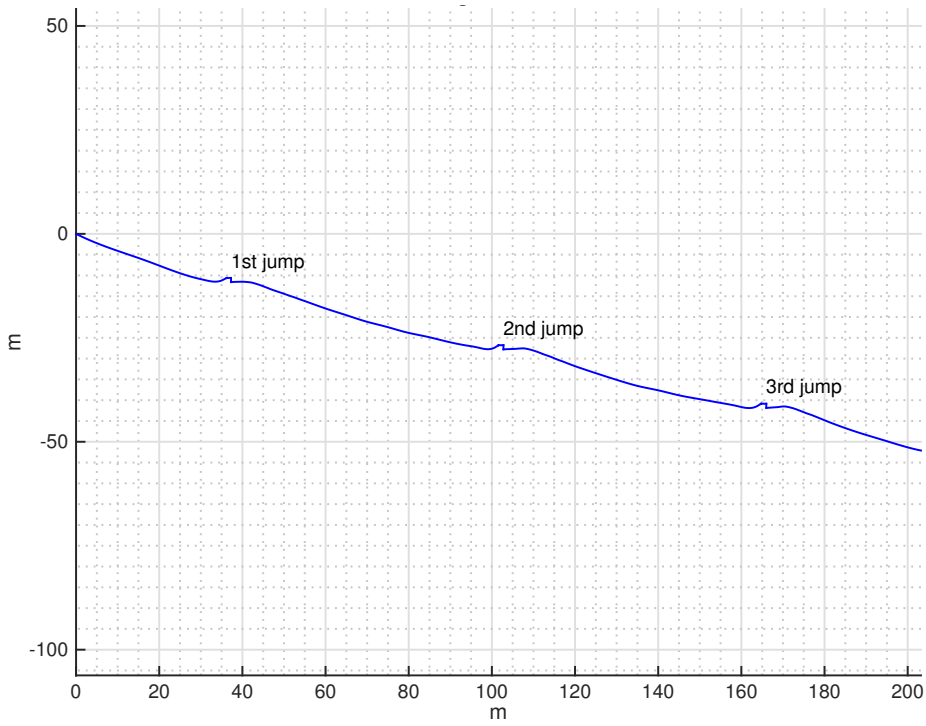


(a) Park profile

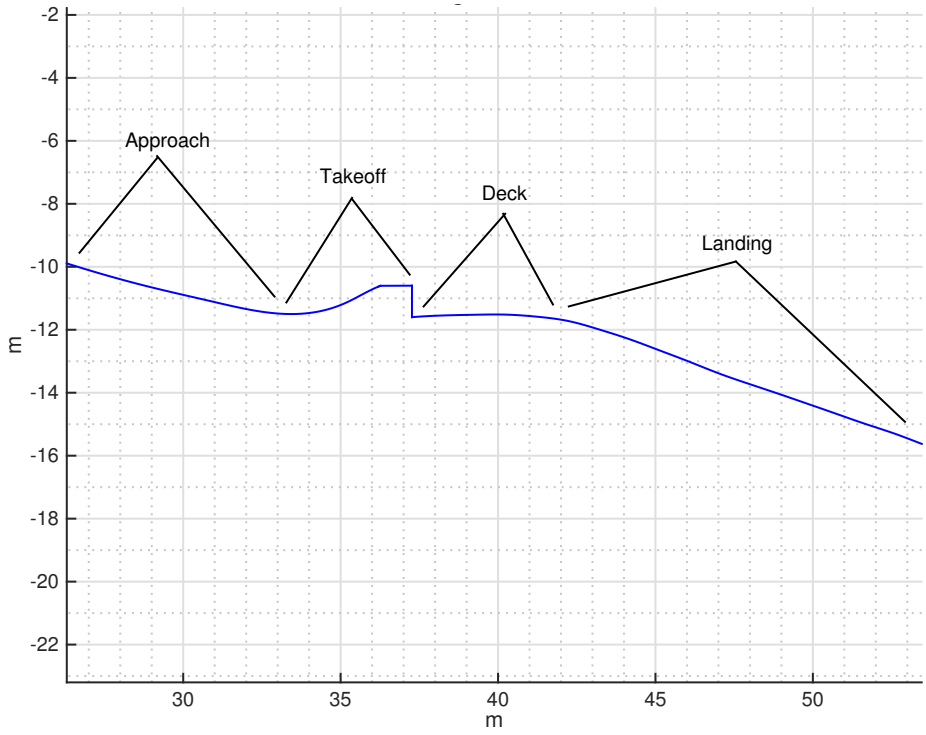


(b) Jump zoom

Figure 24: Tognola Park

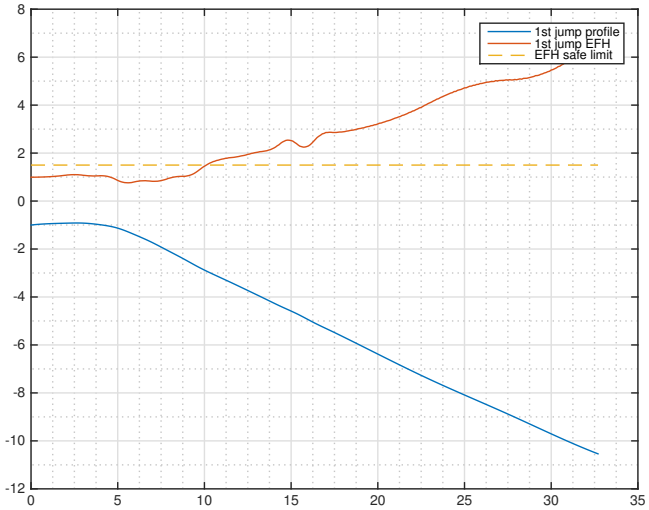


(a) $1^{st}$ jump

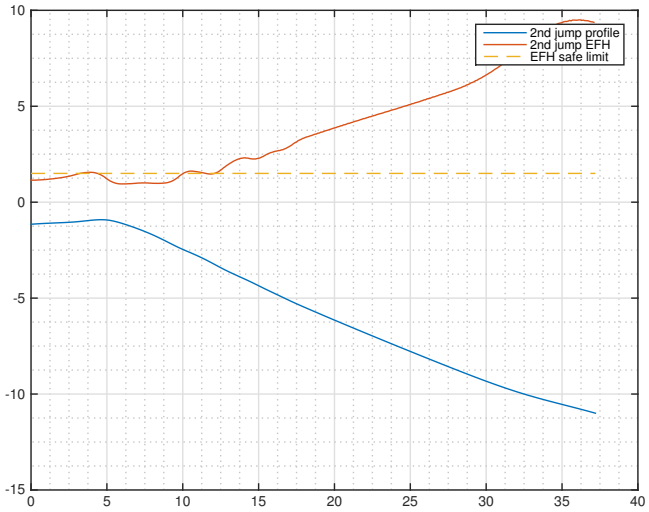


(b) $2^{nd}$ jump

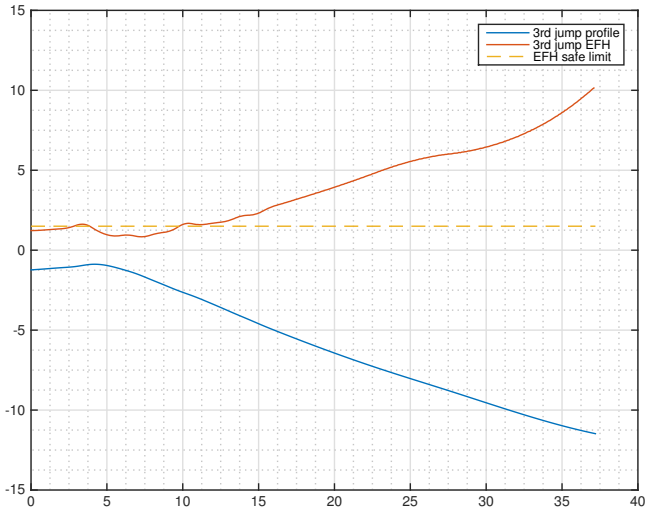


(c) $3^{rd}$ jump

Figure 25: Tognola Park EFH

# 8 Results

As shown by laboratory's results, the $EFH$s evaluated by using the accelerometers are not always comparable neither to those evaluated by using the dynamometric platform nor to those measured by using the motion capture system. This fact probably occurs for many different reasons. First of all, any jump is a perfectly inelastic impact. Since the measurements concerns what happens after the landing, instead of the $EFH$'s definition obtained from the conservation of the energy before the landing, is necessary to dissipate all the energy. On the contrary, some energy is involved in the system's rebound and cushion. In addition, the acceleration is not exactly $g$ but it is affected by any slight body's movement. Hence, this kind of jump is not a real free fall. Another relevant factor regards the model used. Since the momentum of the centre of mass is conserved, it would be worthwhile to estimate the body's centre of mass.

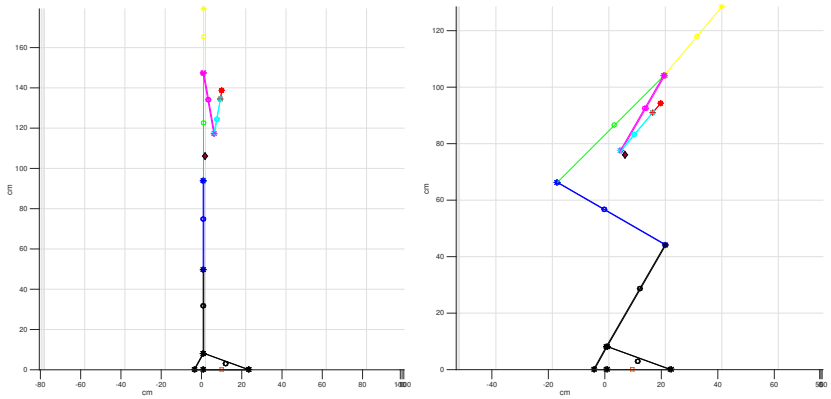

(a) Stand position, arms folded (b) Flex position, arms folded

Figure 26: Dempster human body model without snowboard

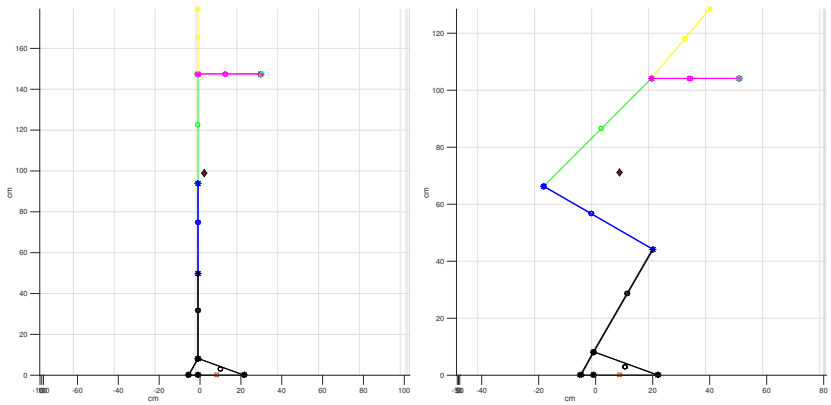

(a) Stand position, forearms folded (b) Flex position, forearms folded

Figure 27: Dempster human body model with snowboard

Figure 26 and Figure 27 ($h = 179\,cm$, $m = 76.4\,kg$, $m_{snow} = 6.7\,kg$) show how much the position of the body's centre of mass (black diamond) is influenced by the posture. The rough approximation of the centre of mass' position and the partial schematisation of the human body could be the reason why the $EFH$s evaluated by using the platform are not always comparable to the accelerometers' results. Therefore, it would be preferable to extend the jump's theoretical treatise to the real body's centre of mass instead of the point-mass assumption. The idealisation would be possible by developing human body's models, as the the Dempster's one, while the measurement could be executed by using inertial sensors, as the $Xsens$. Another problem could be the different acquisition's frequency of the instrumentation. The in field test session seems to yield more precise results. In this case, the principal cause of imprecision is probably due to the individuation of the acceleration perpendicular to the surface. In conclusion, also the momentum of inertia of the body, the skin and soft tissues' effect and the board's lever arm effect (the accelerometer was not applied on the board's centre) have not been evaluated. Indeed, in a terrain park's jump, the rider rotates himself in order to better control the landing. Despite these imprecisions, the experimental tests apparently follow the awaited theoretical's hypothesis .

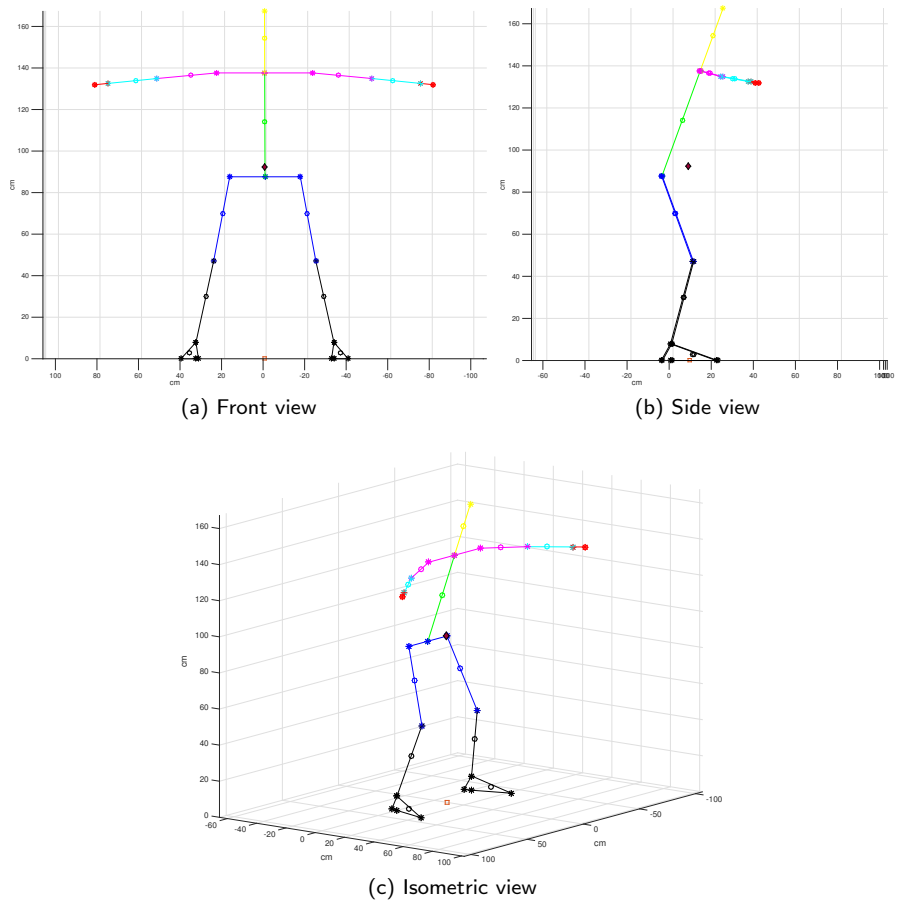

(a) Front view

(b) Side view

(c) Isometric view

Figure 28: Dempster human body model for the in field session

# 9 Conclusion

In the light of these evidences, an in-depth analysis is definitely required to achieve undeniable results. Since the profiles' geometrical behaviour adequately reflect the theory, is necessary to completely understand what happens during the motion. First of all, proceeding to evaluate every possible source of error is essential. This procedure allows to choose the best model to be implemented among all the suitable ones. Furthermore, it permits to validate the approximations adopted. Once this method will be sufficiently proven, it will be worthy to analyse the other approximations such as the omission of the uncontrollable factors. These factors could be the dissipative and aerodynamic forces, the jumper's 'pop' velocity, the jumper's behaviour beneath and beyond the takeoff, the atmospheric agents and the profile's conservation during time. Moreover, another fundamental cause of injury to be considered is the inverse spin and every kind of rotation which a jumper can perform. These can be executed either on purpose or accidentally. Even if the rider independently chooses to perform an air trick, it is not given for granted that everything is always under his control. For this reason it would be appropriate to manage the $EFH$ for any landing scenario. Perhaps, it could be advantageous to adjust the safety's features and design with respect to the users' level and their performances. Another arduous hurdle to overcome is the proposal of protocols and standards, which is necessary to spread a scientific method of design. Finally, definitely less essential and perhaps more difficult, it is to achieve the consumers' suitable feedback. It should be noticed that the users' interest and appreciation will not probably be as high as desirable. This is due to the lack of risk's perception because of the absence of the hollow below the jumper's feet. Possibly, the more precisely the profile can be managed the more the jump's characteristics can safely satisfy the users' desires.

# A Appendix - Data and graphs

## A.1 One accelerometer

### A.1.1 1 trial

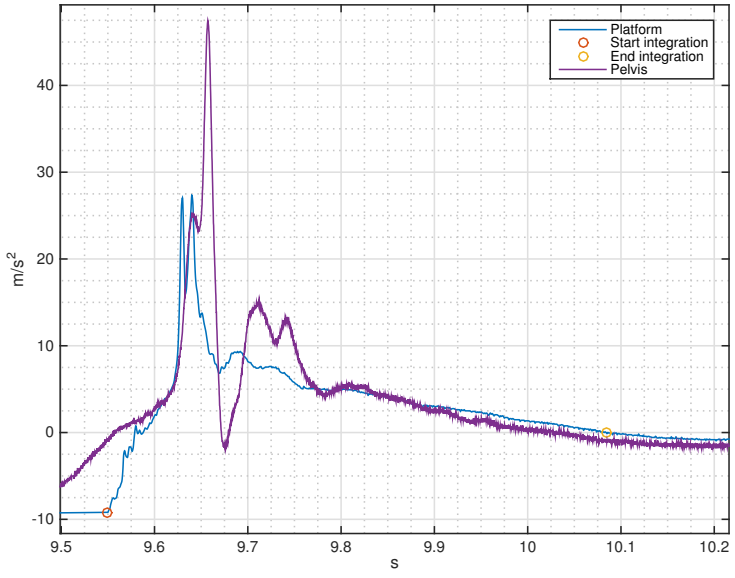


(a) Acceleration

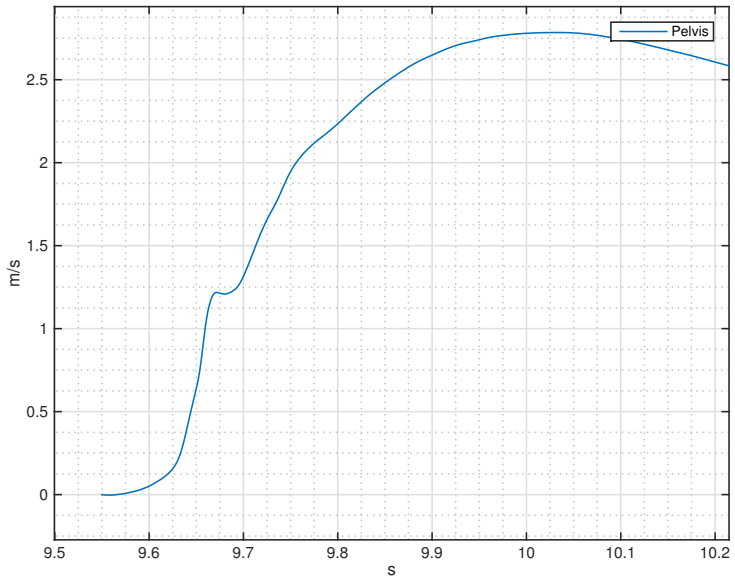


(b) Velocity

### A.1.2 2 trial

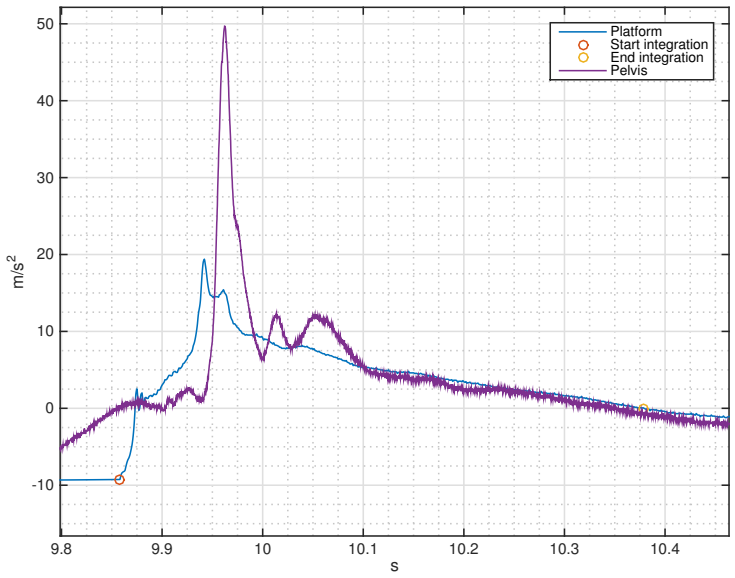


(a) Acceleration

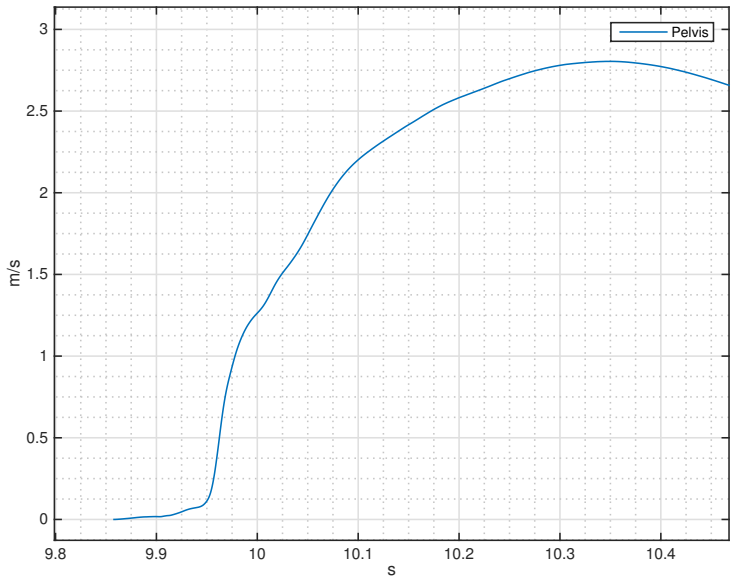


(b) Velocity

### A.1.3 3 trial

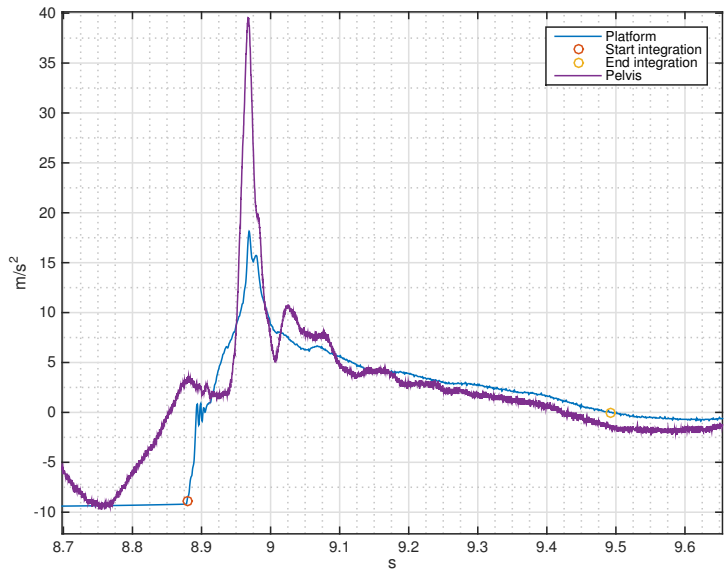


(a) Acceleration

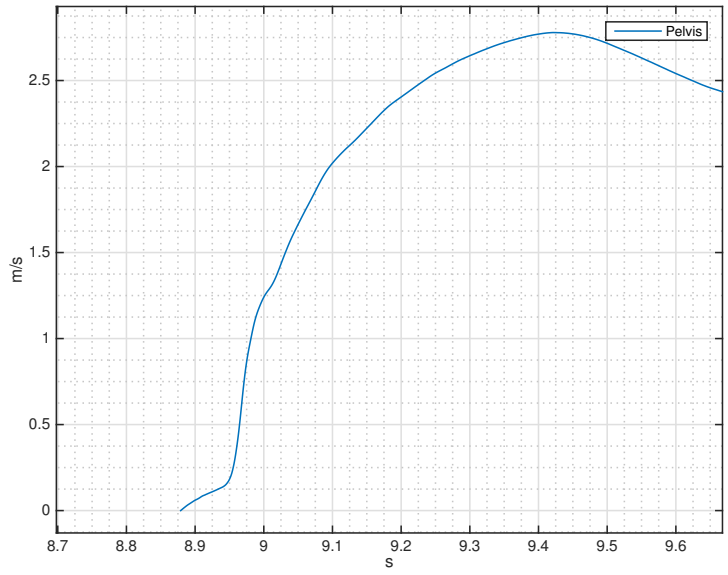


(b) Velocity

### A.1.4 4 trial

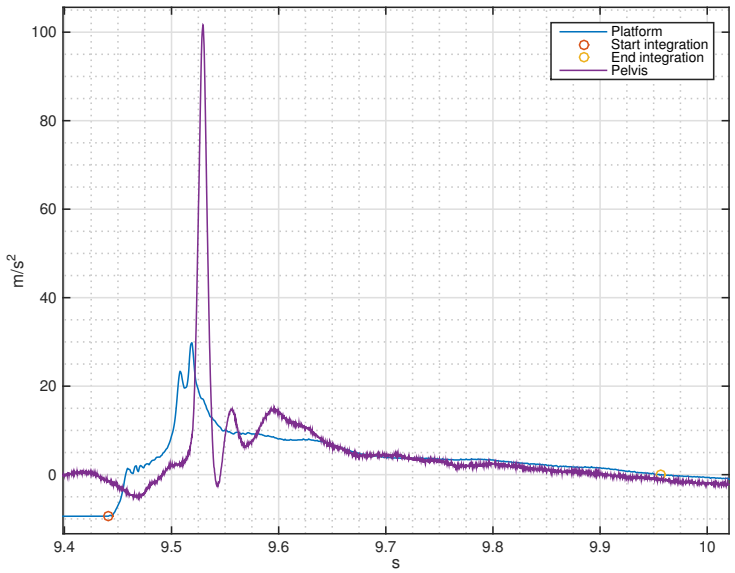


(a) Acceleration

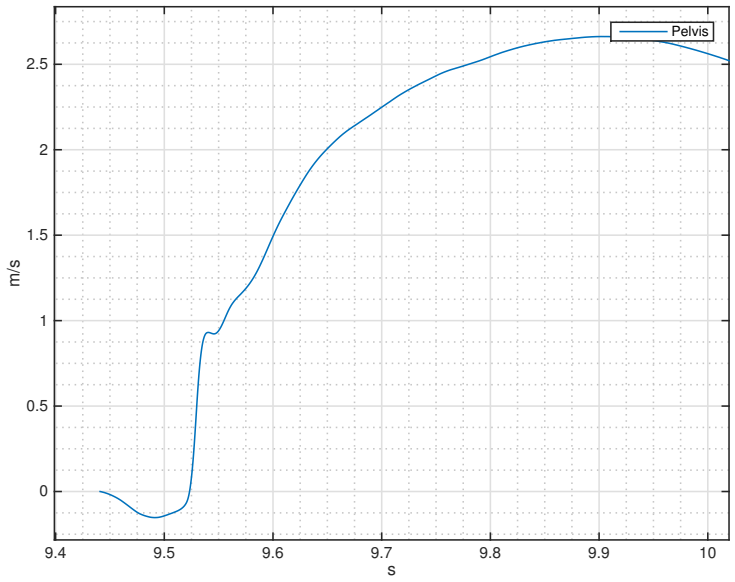


(b) Velocity

### A.1.5 5 trial

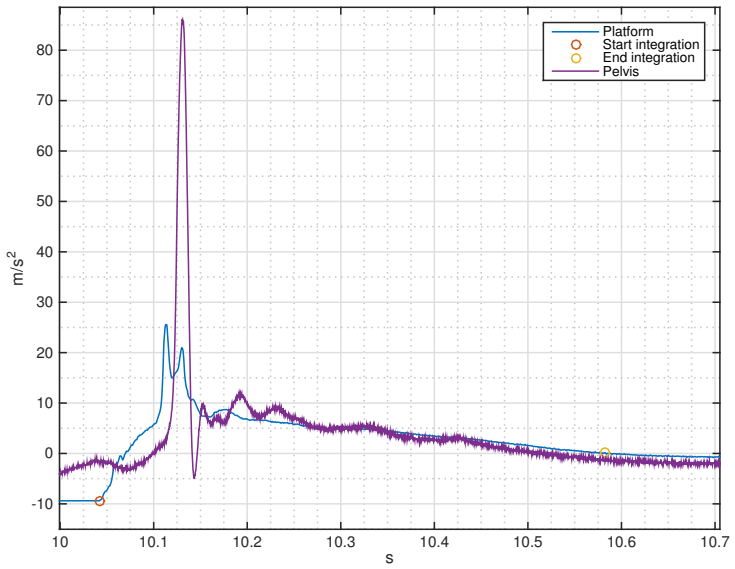


(a) Acceleration

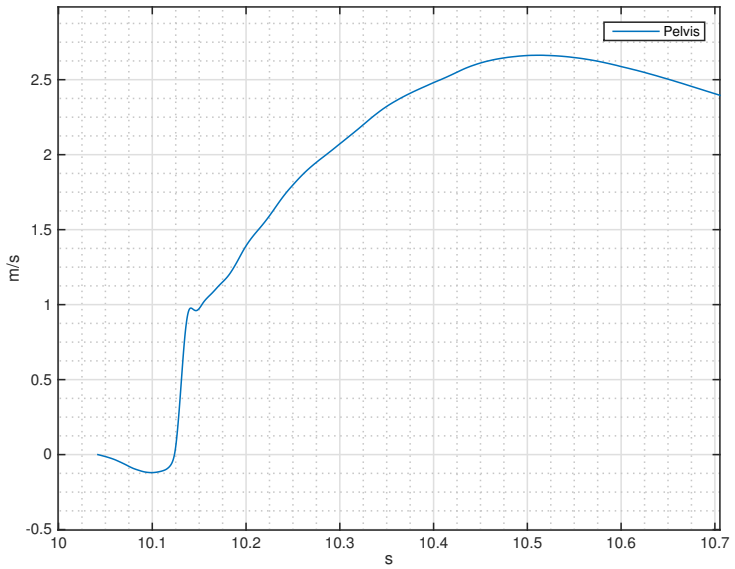


(b) Velocity

### A.1.6 6 trial

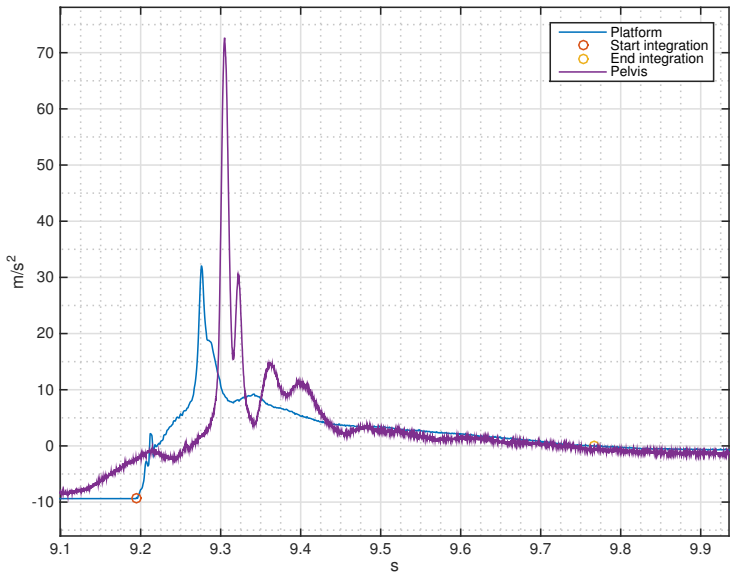


(a) Acceleration

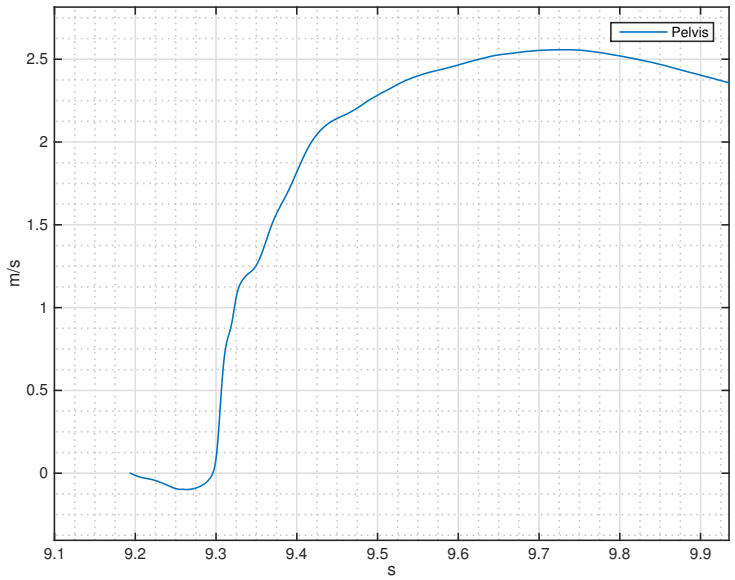


(b) Velocity

### A.1.7 7 trial

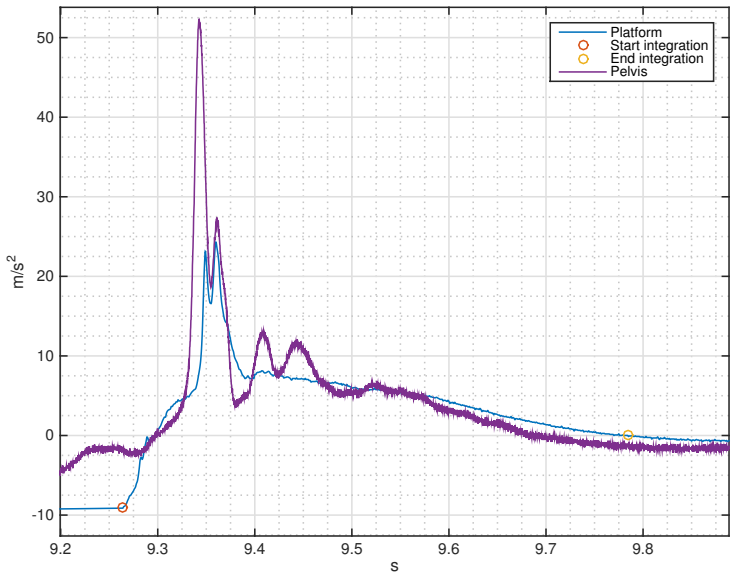


(a) Acceleration

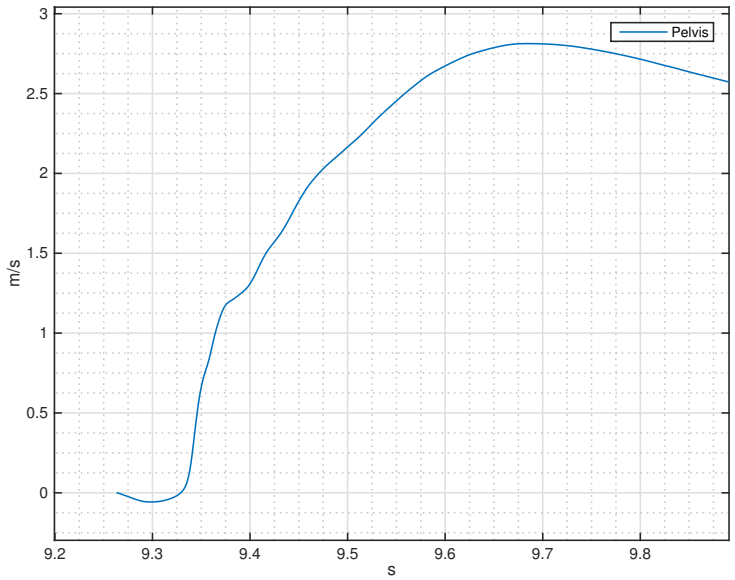


(b) Velocity

### A.1.8 8 trial

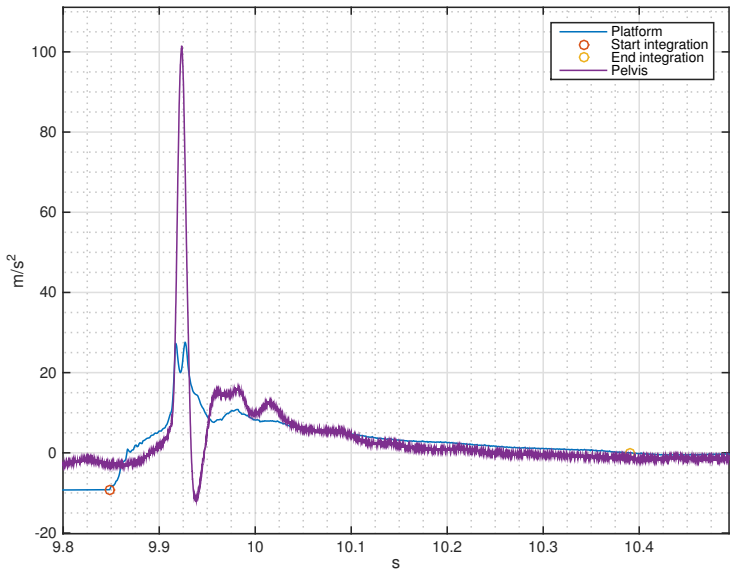


(a) Acceleration

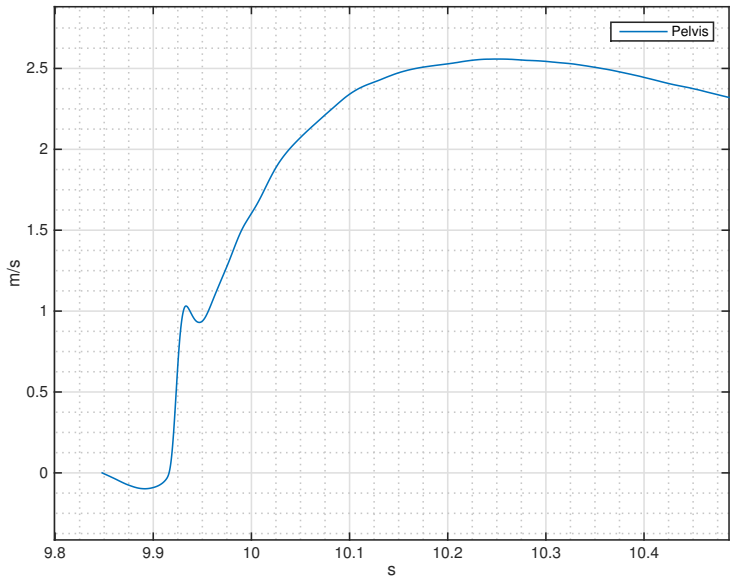


(b) Velocity

### A.1.9 9 trial

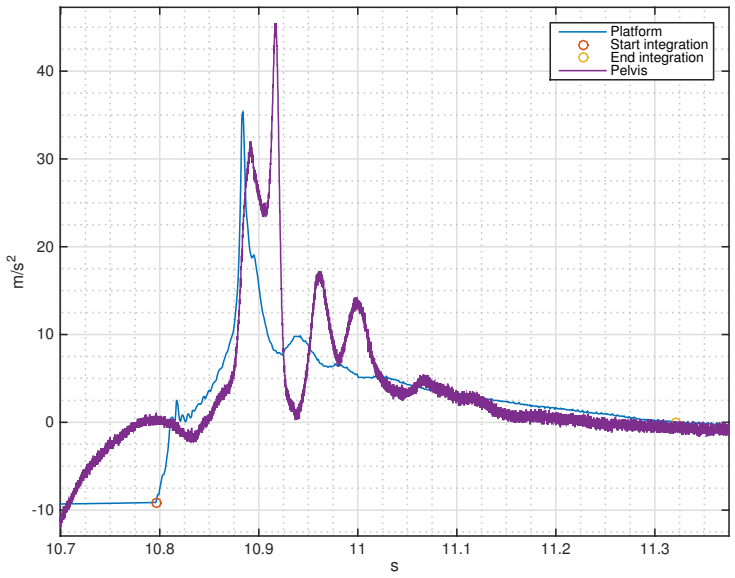


(a) Acceleration

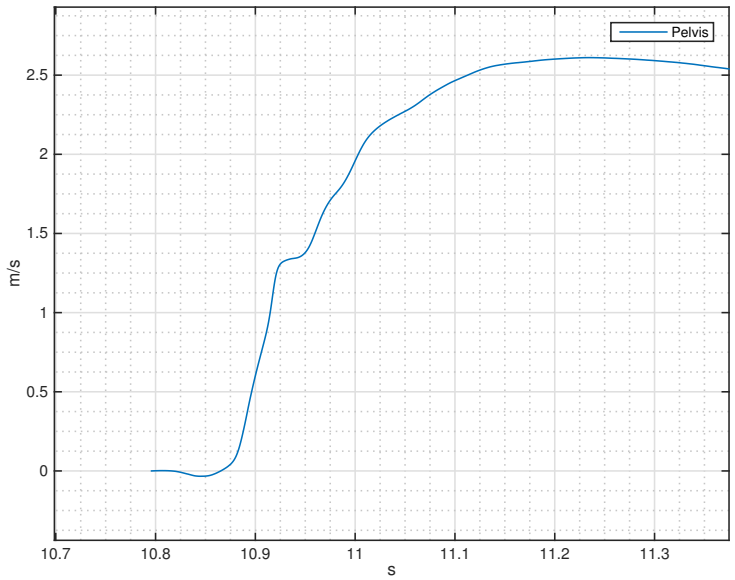


(b) Velocity

### A.1.10 10 trial

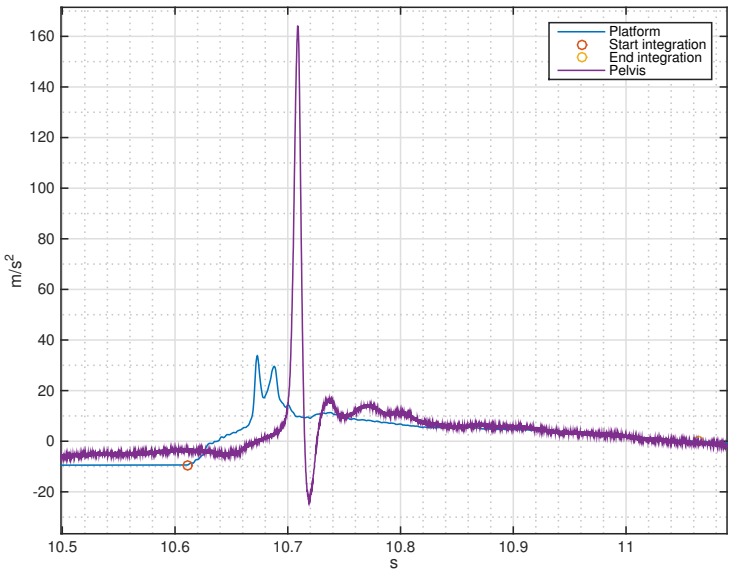


(a) Acceleration

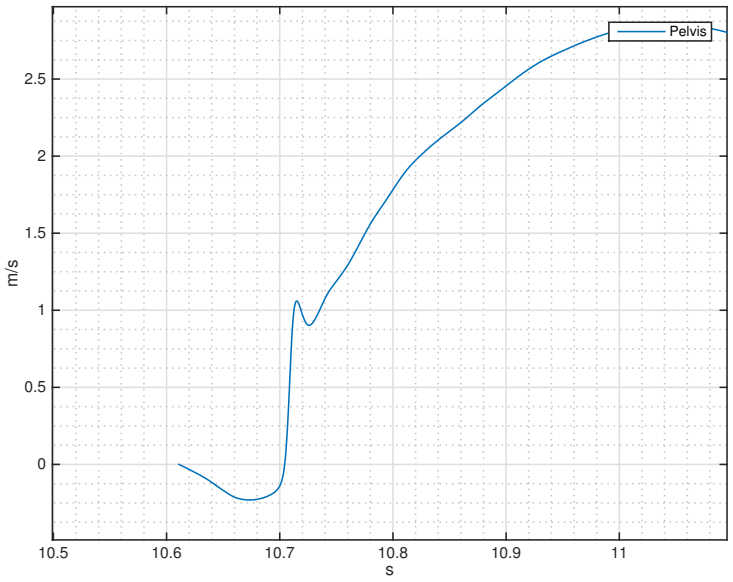


(b) Velocity

### A.1.11 11 trial

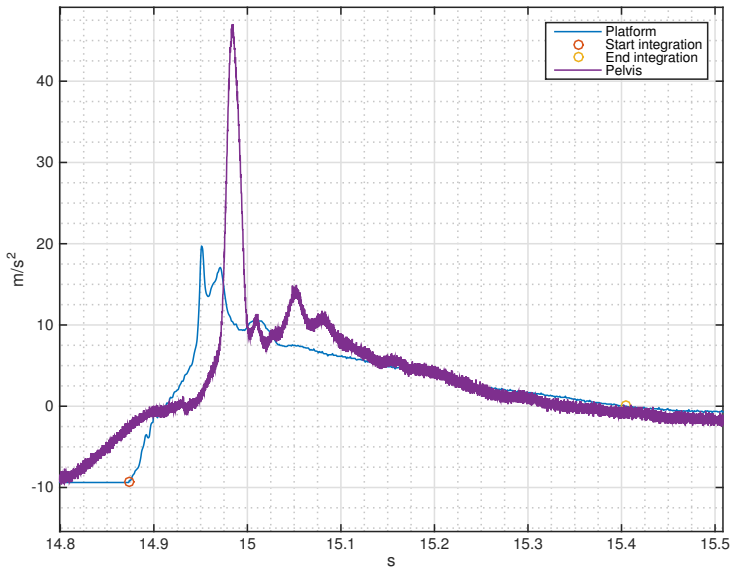


(a) Acceleration

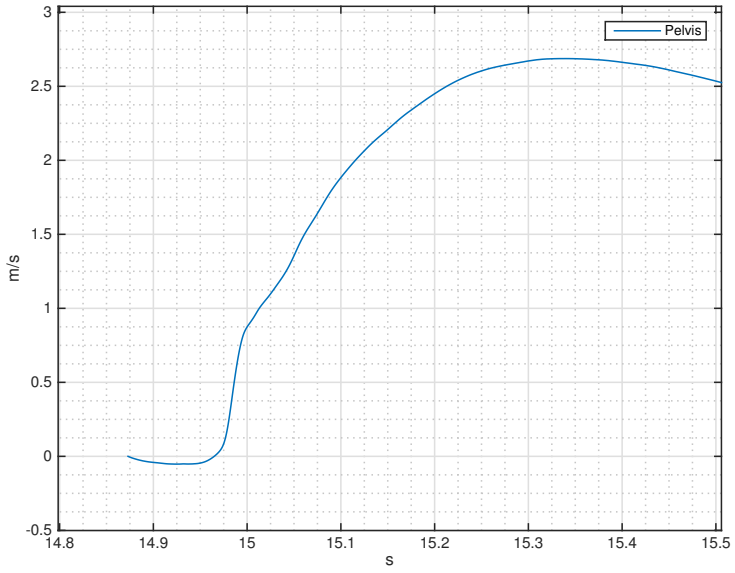


(b) Velocity

### A.1.12 12 trial

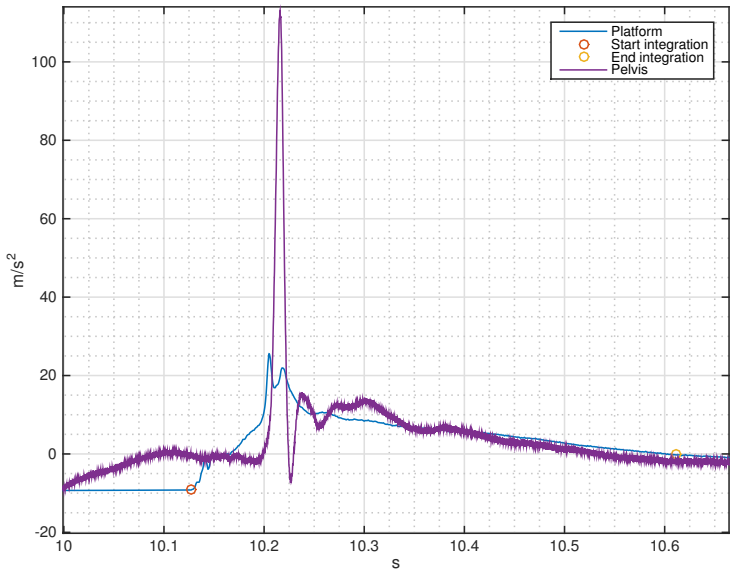


(a) Acceleration

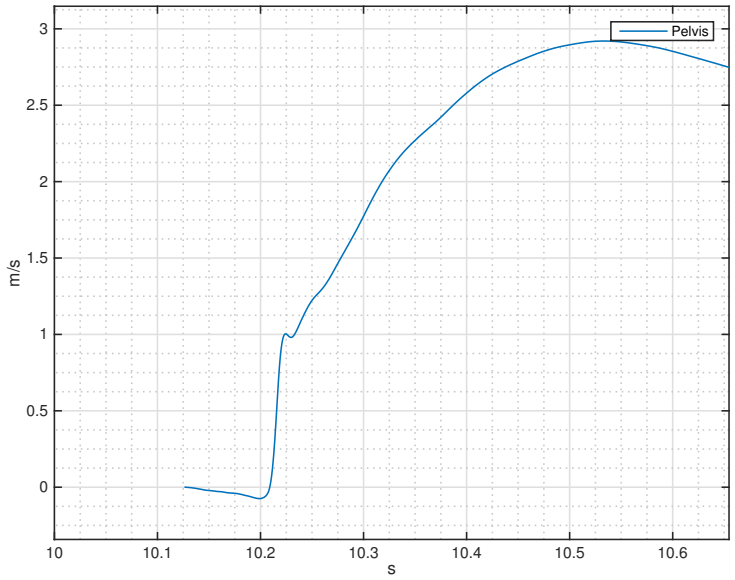


(b) Velocity

## A.2 Two accelerometers

### A.2.1 1 trial

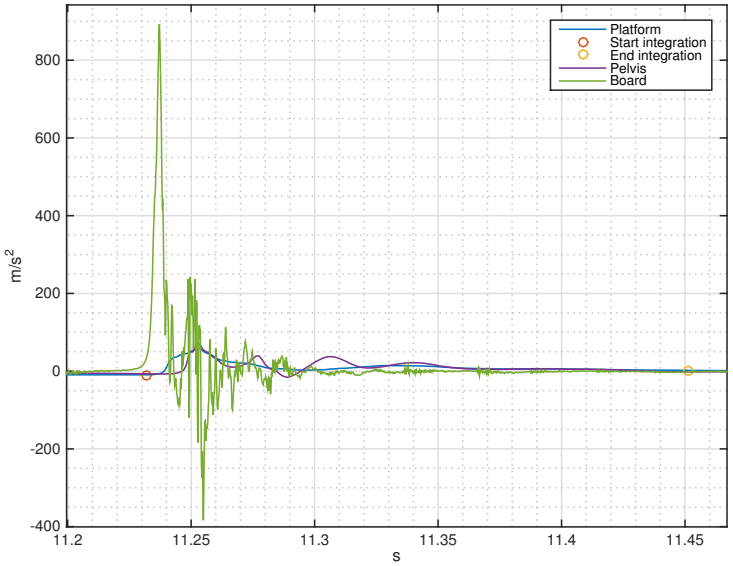


(a) Acceleration

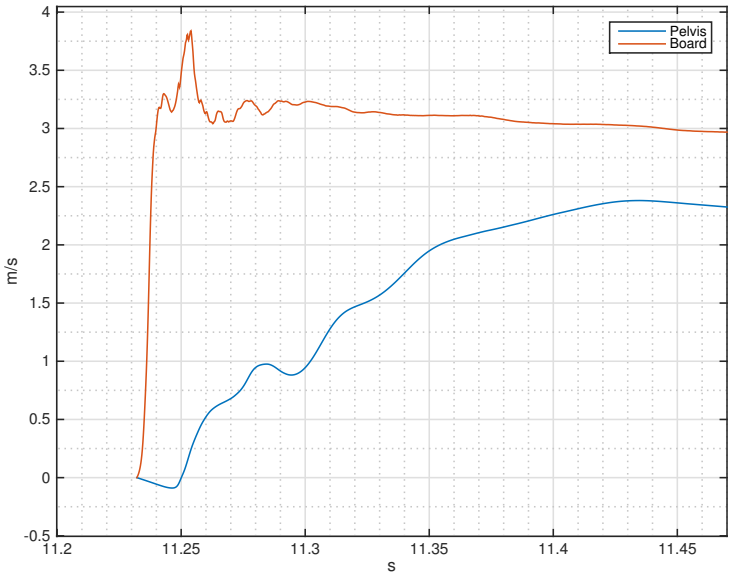


(b) Velocity

### A.2.2 2 trial

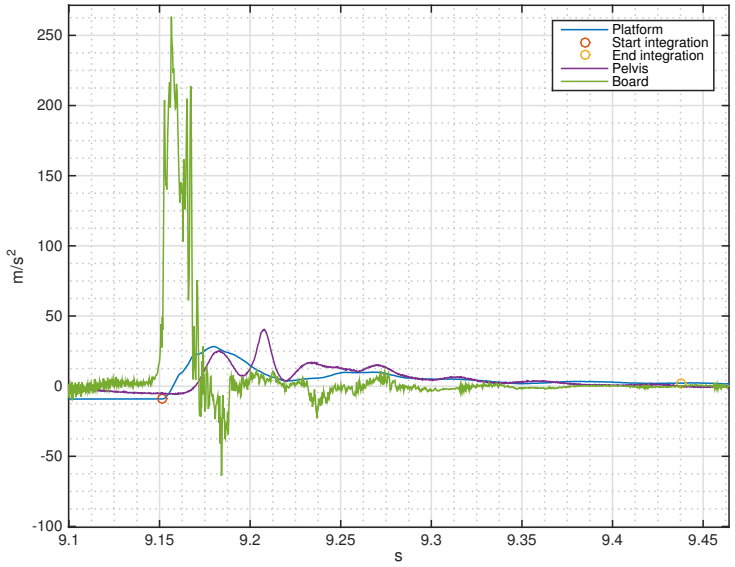


(a) Acceleration

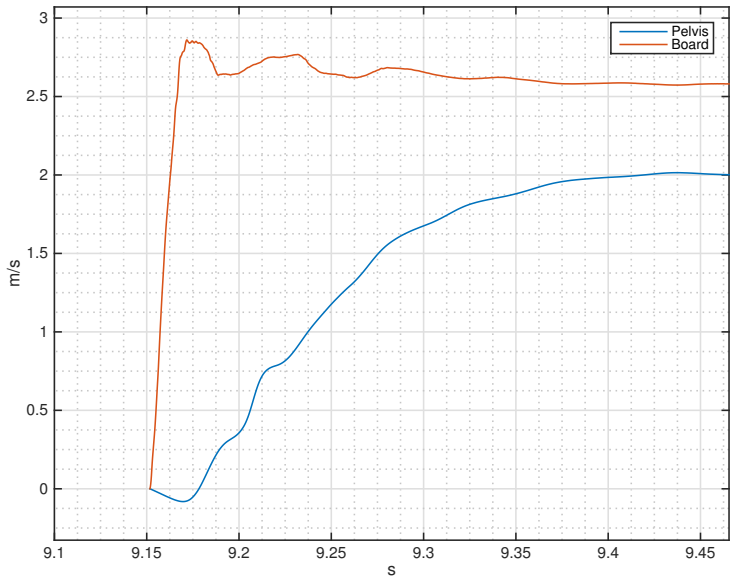


(b) Velocity

### A.2.3 3 trial

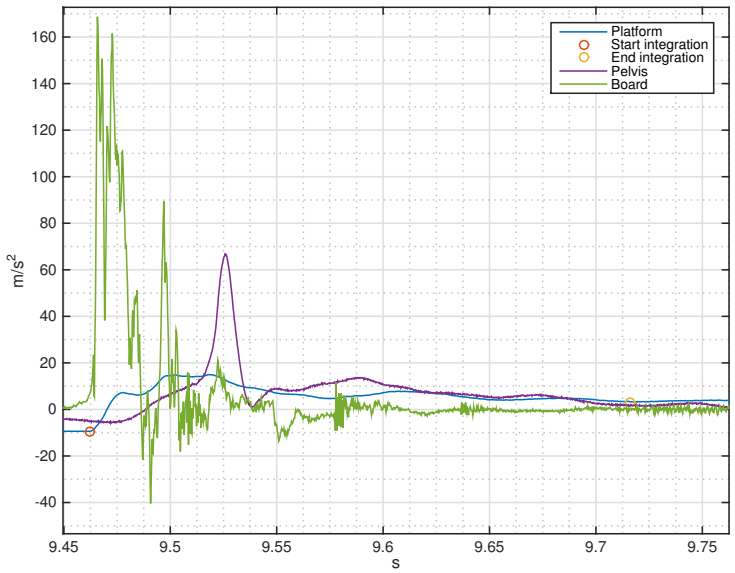


(a) Acceleration

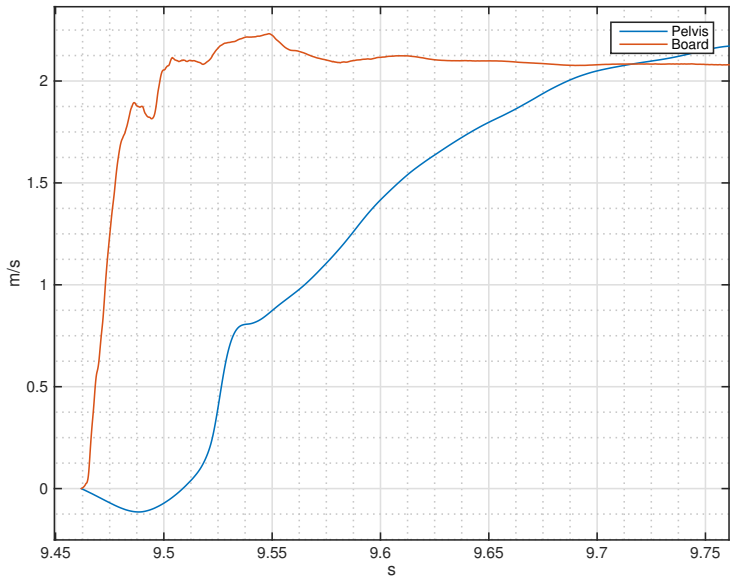


(b) Velocity

### A.2.4 4 trial

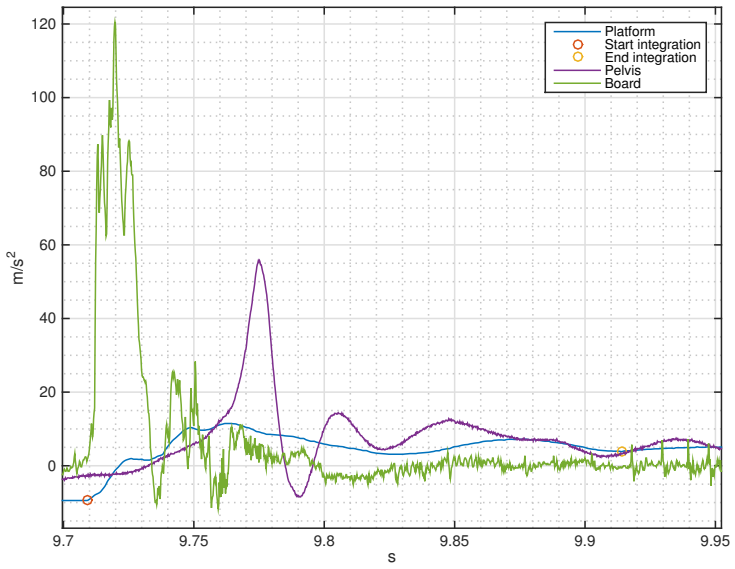


(a) Acceleration

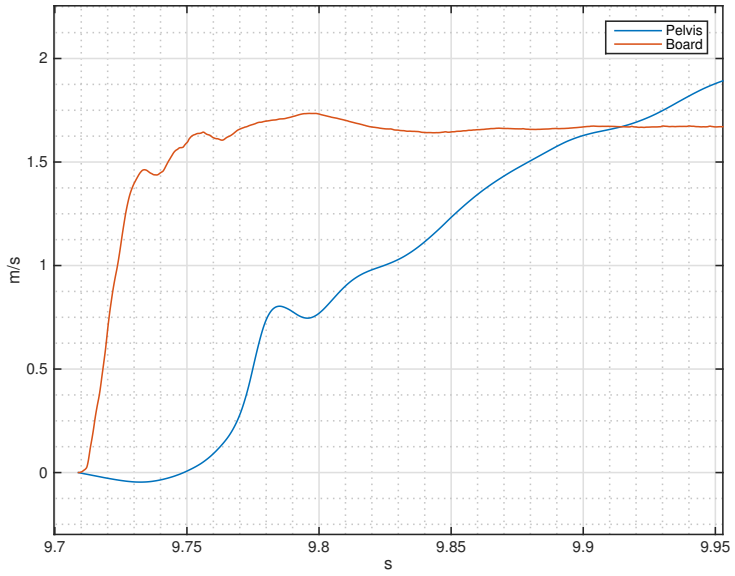


(b) Velocity

### A.2.5 5 trial

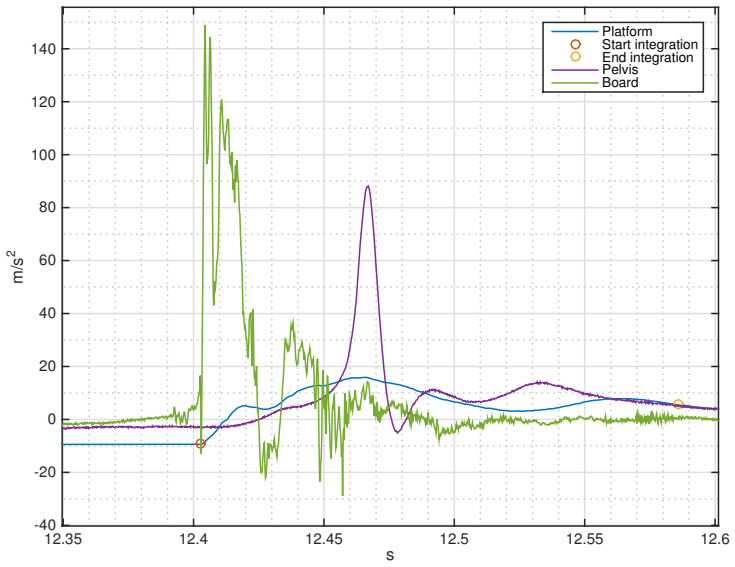


(a) Acceleration

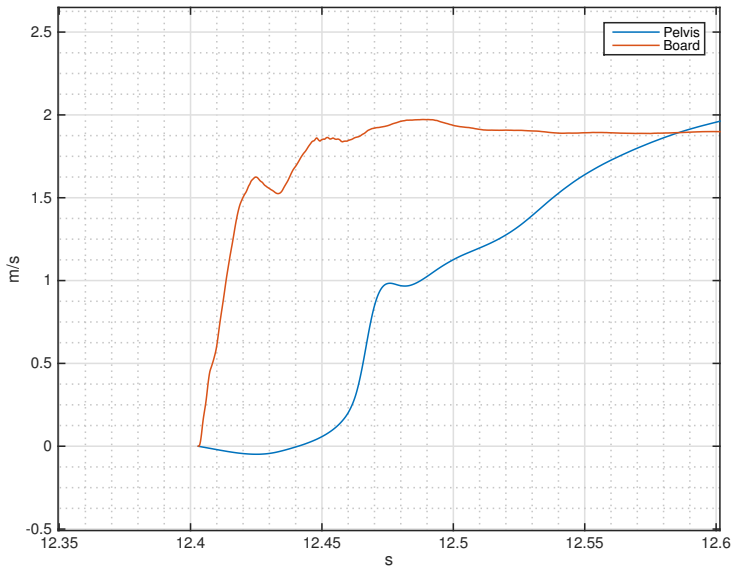


(b) Velocity

### A.2.6 6 trial

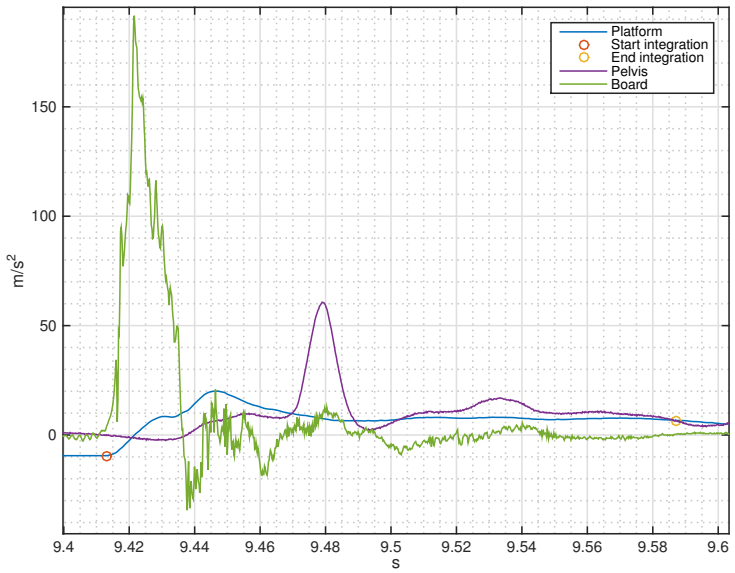


(a) Acceleration

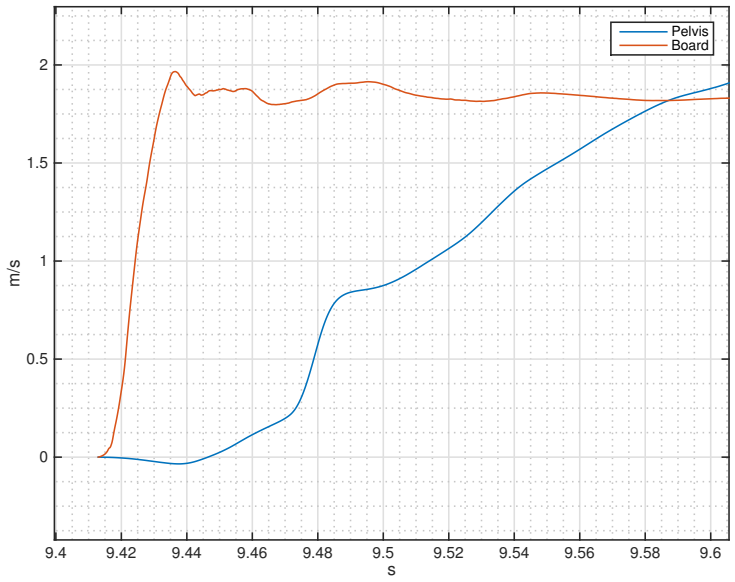


(b) Velocity

### A.2.7 7 trial

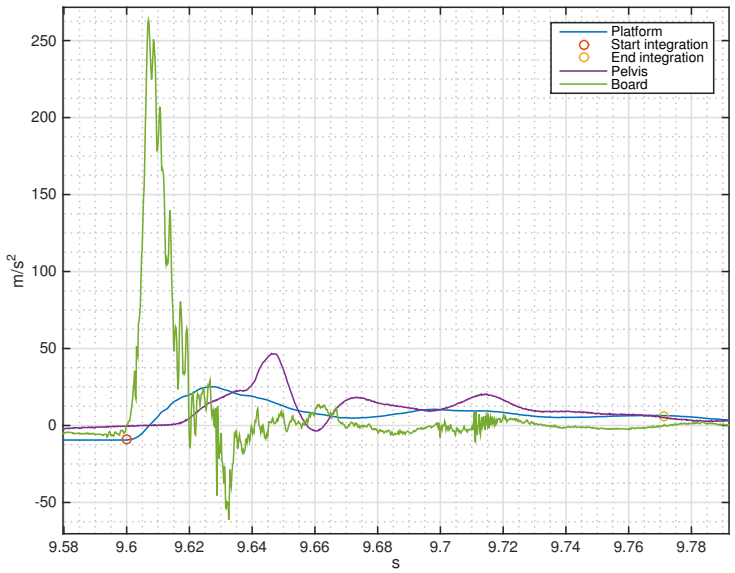


(a) Acceleration

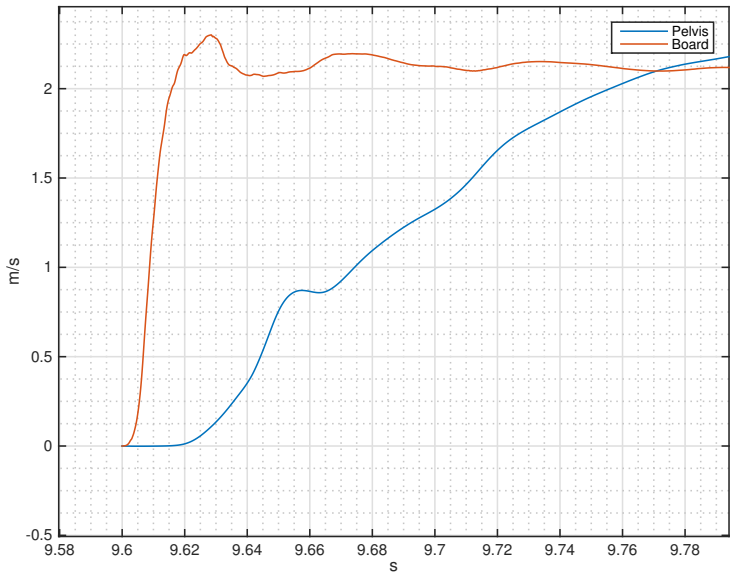


(b) Velocity

### A.2.8 8 trial

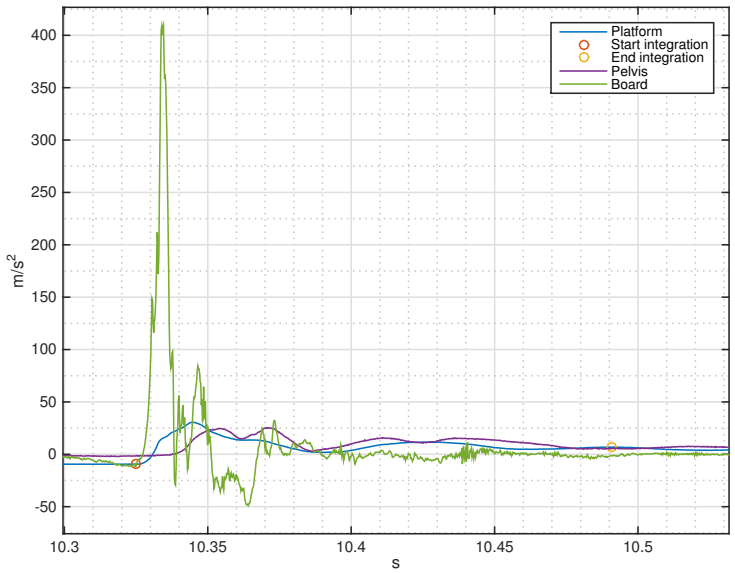


(a) Acceleration

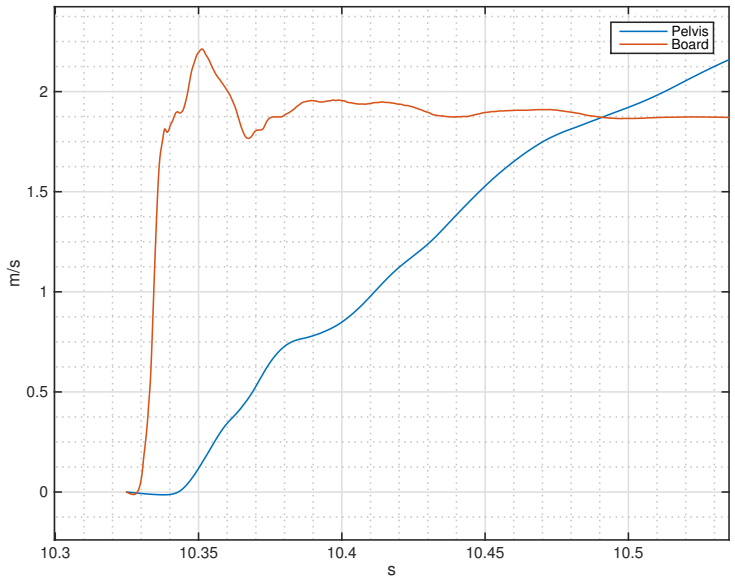


(b) Velocity

### A.2.9 9 trial

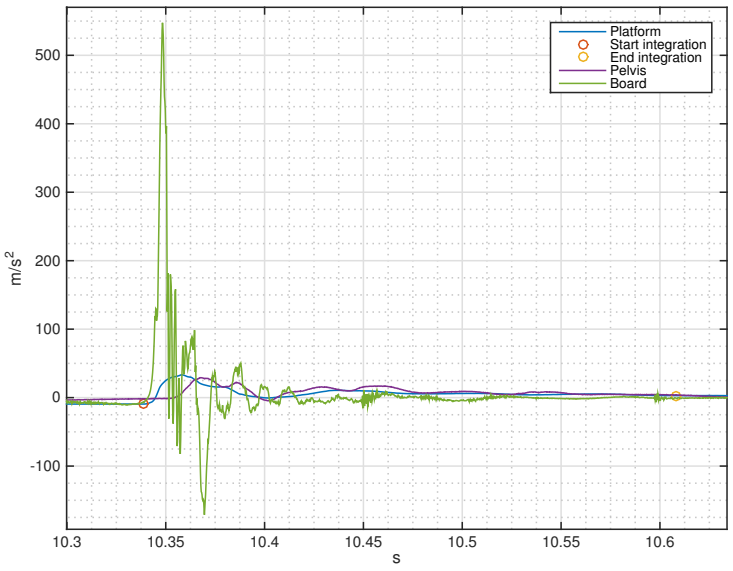


(a) Acceleration

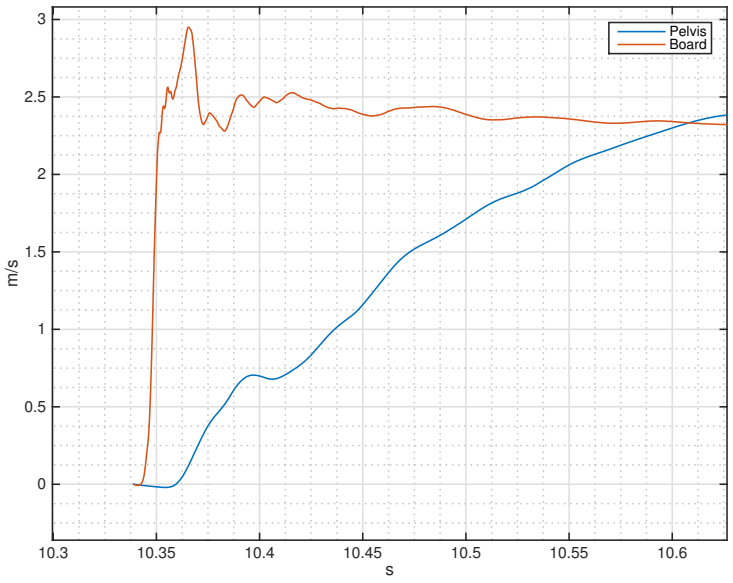


(b) Velocity

### A.2.10 10 trial

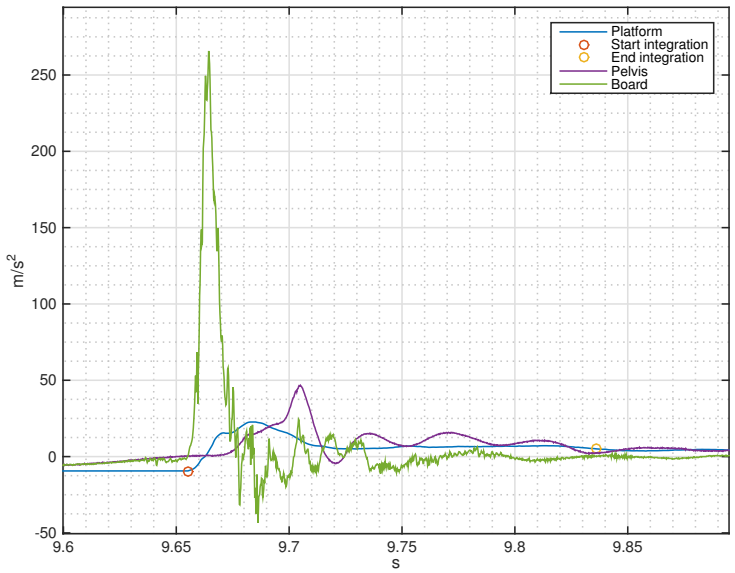


(a) Acceleration

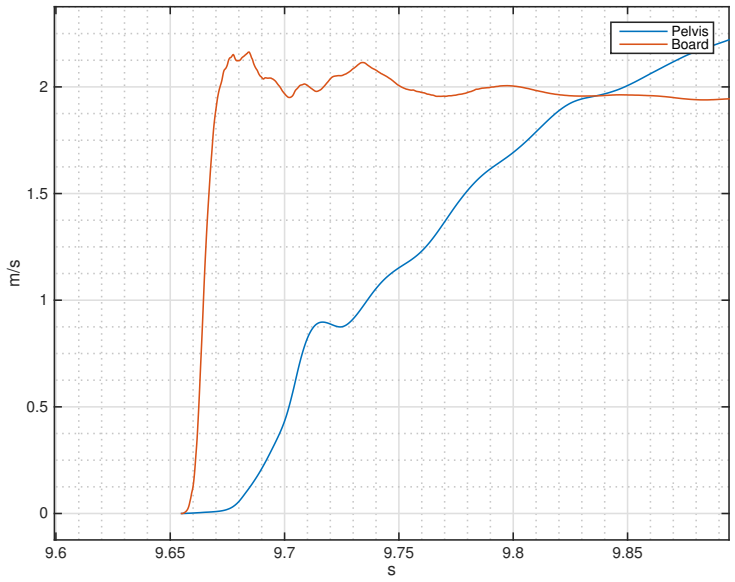


(b) Velocity

### A.2.11 11 trial

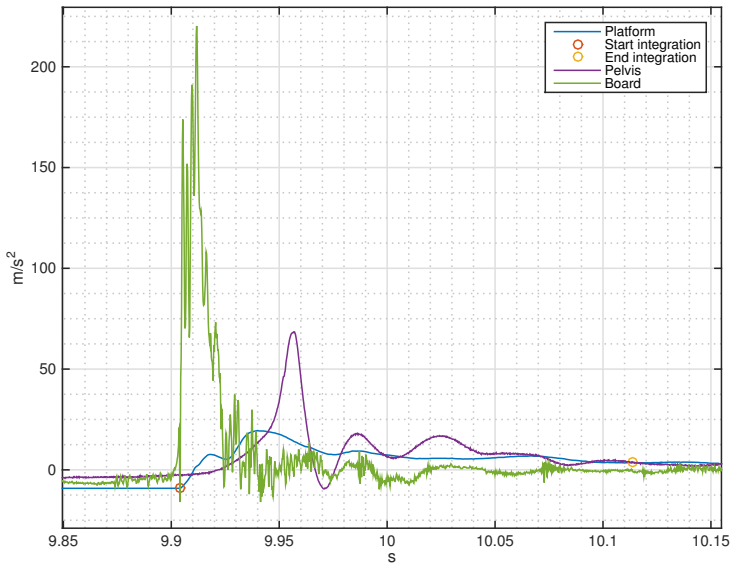


(a) Acceleration

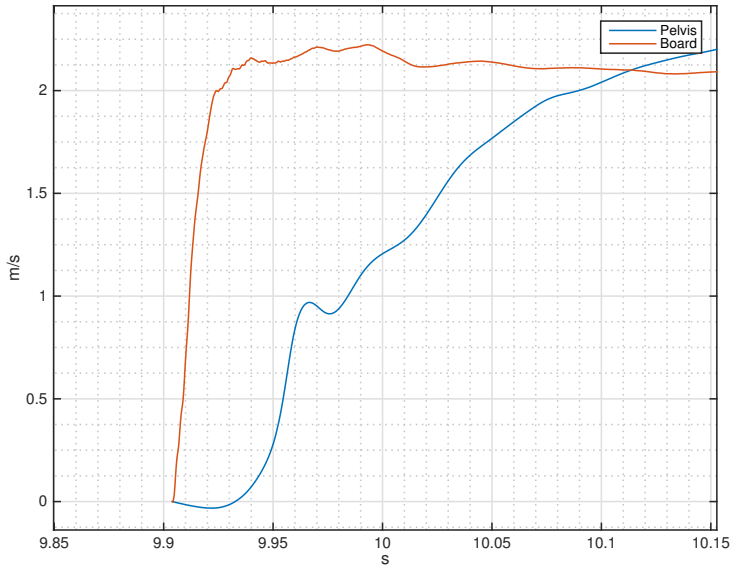


(b) Velocity

### A.2.12 12 trial

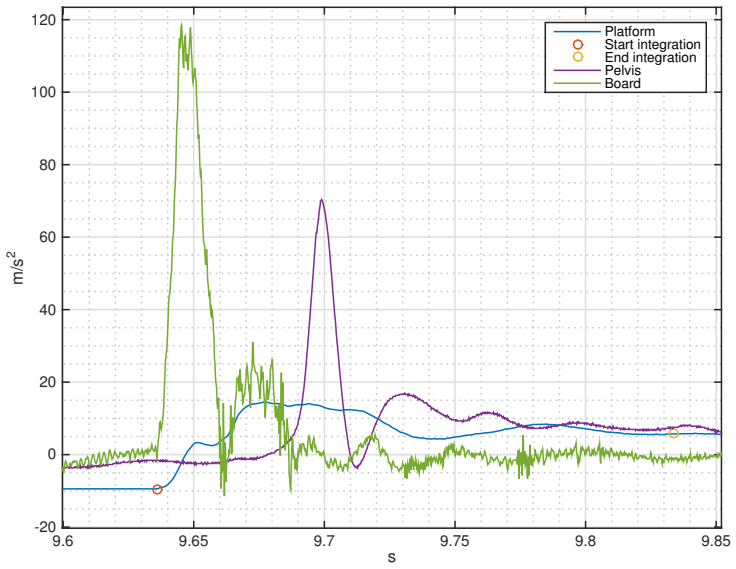


(a) Acceleration

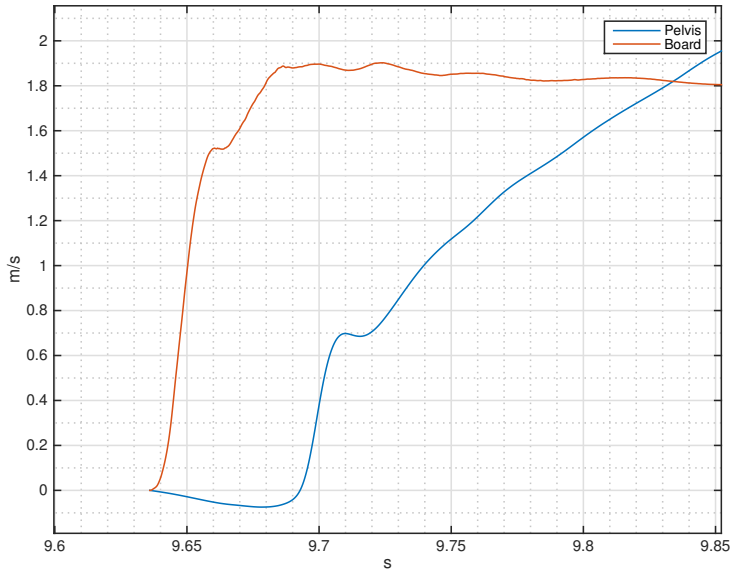


(b) Velocity

## A.3 In field

### A.3.1 1 trial

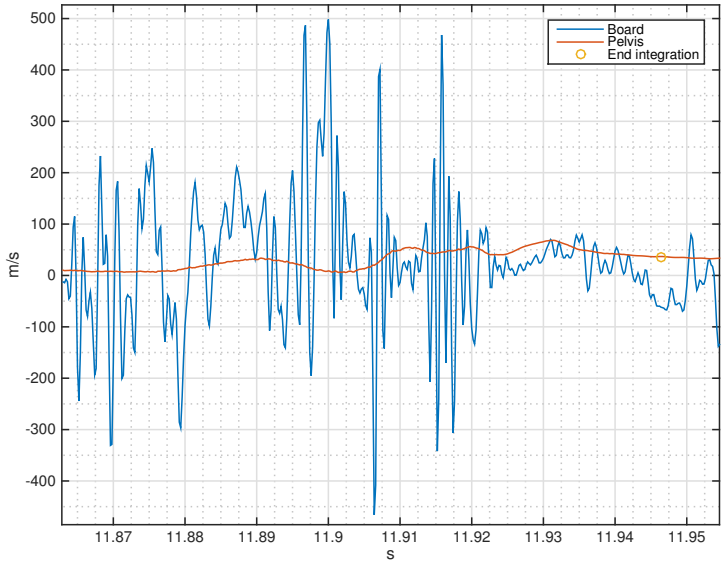


(a) Acceleration

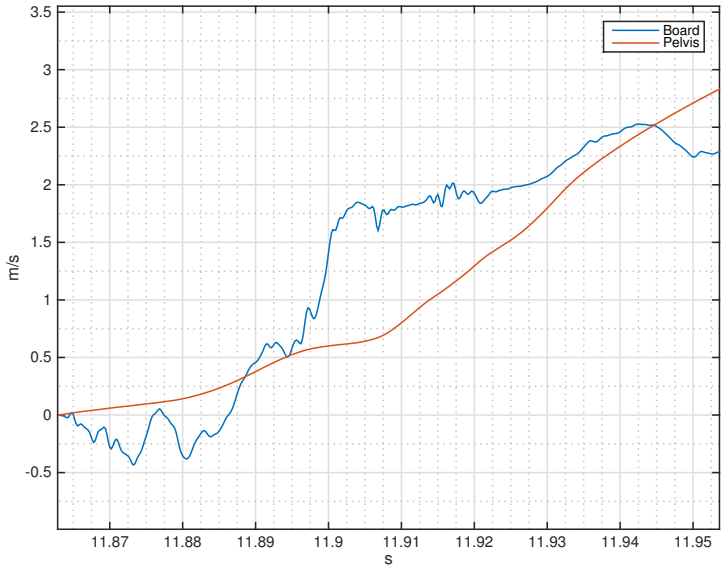


(b) Velocity

### A.3.2 2 trial

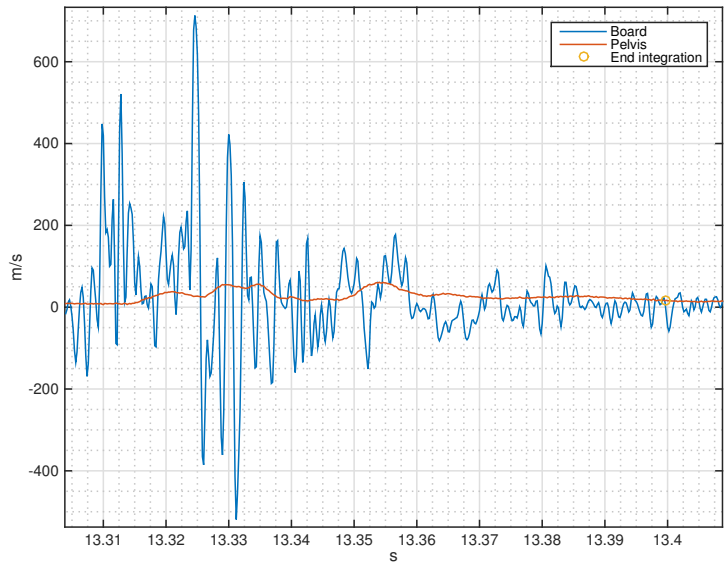


(a) Acceleration

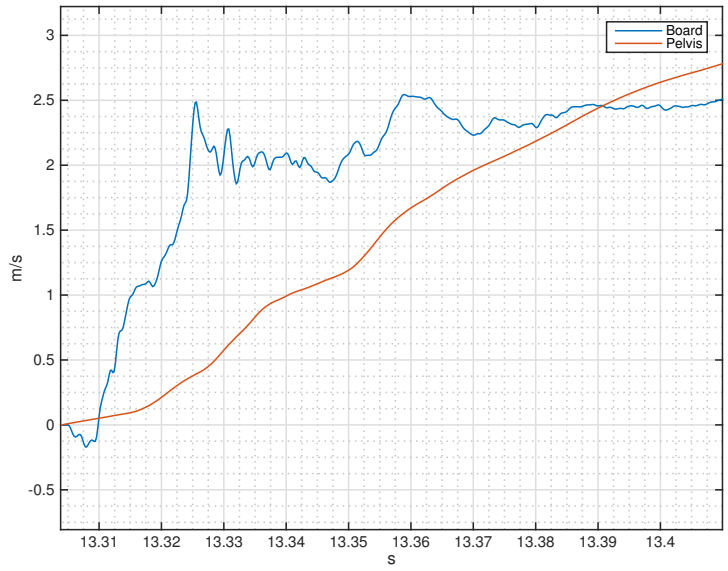


(b) Velocity

### A.3.3 3 trial

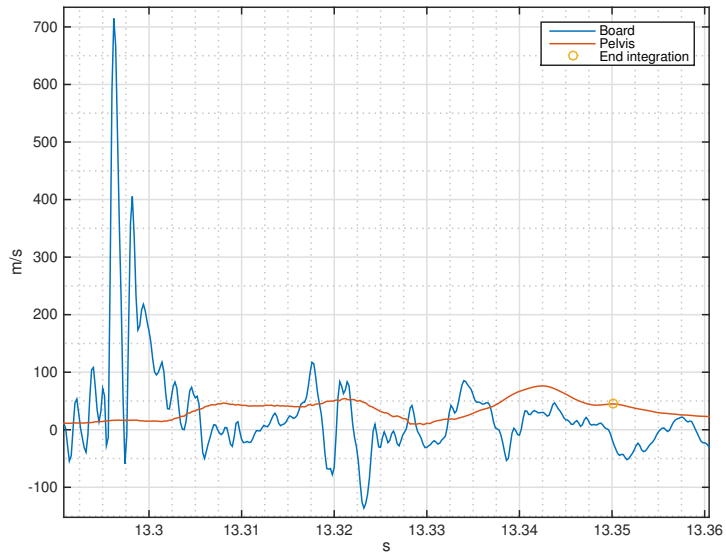


(a) Acceleration

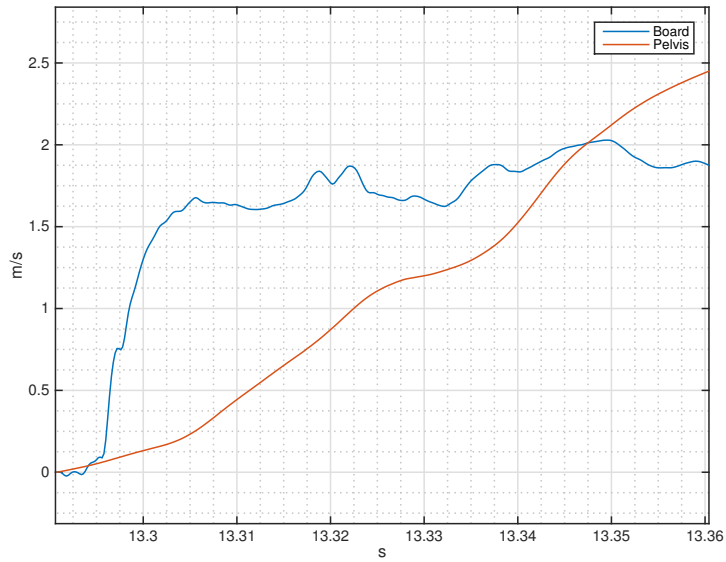


(b) Velocity

### A.3.4 4 trial

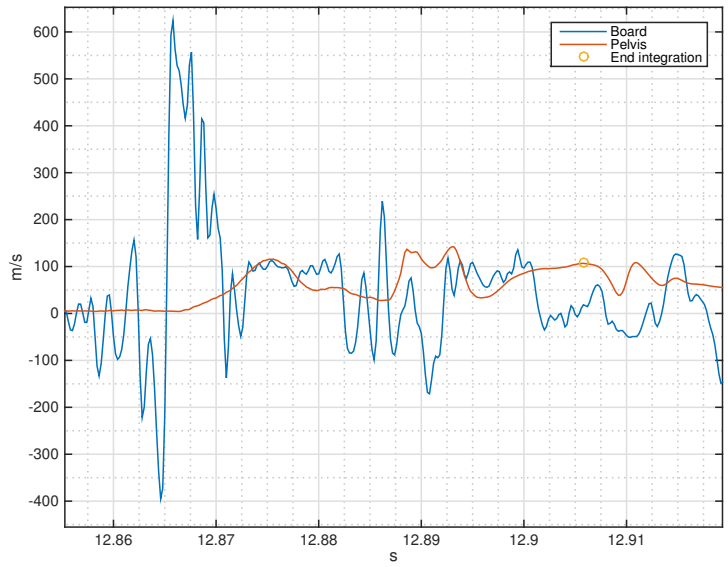


(a) Acceleration

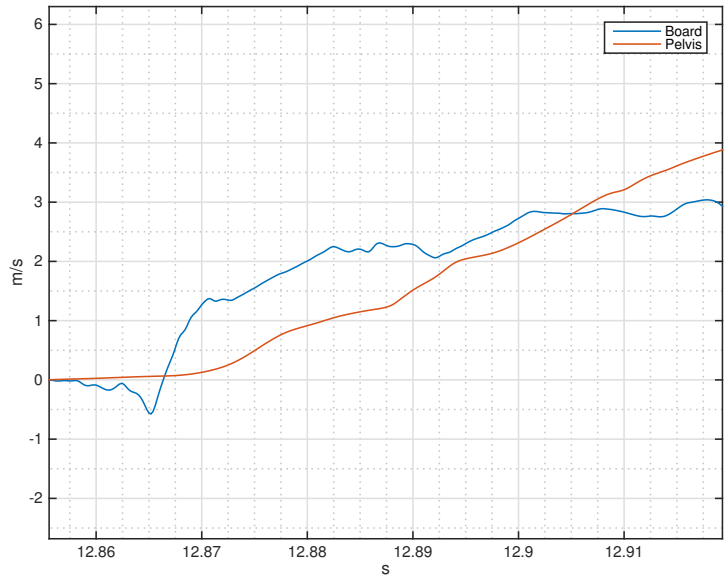


(b) Velocity

### A.3.5 5 trial (FALL)

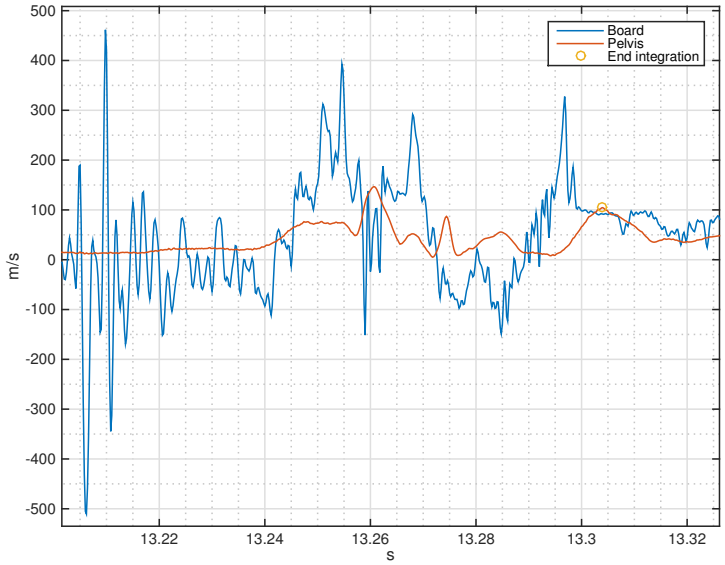


(a) Acceleration

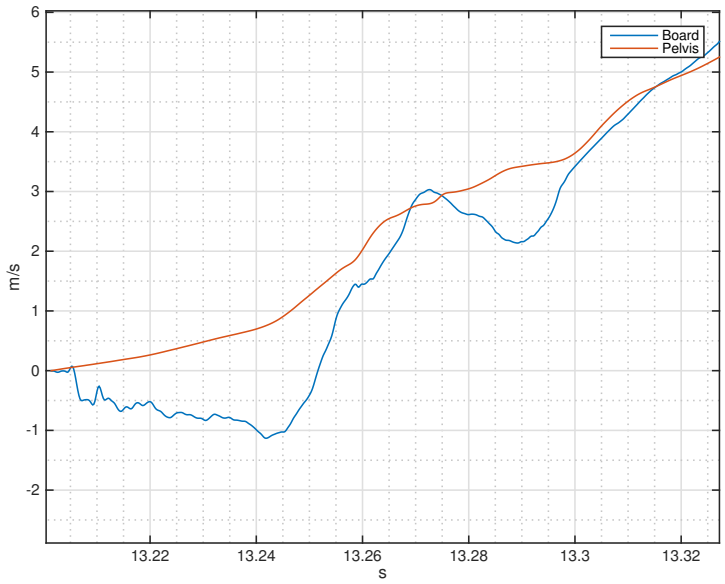


(b) Velocity

### A.3.6 6 trial

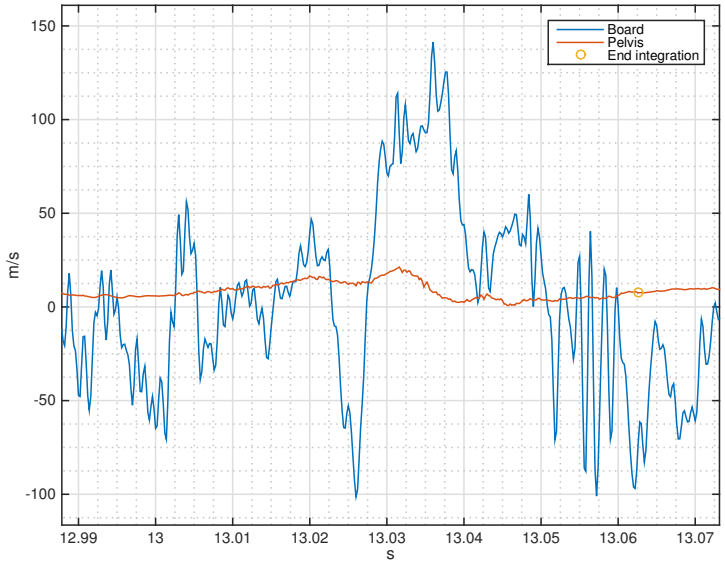


(a) Acceleration

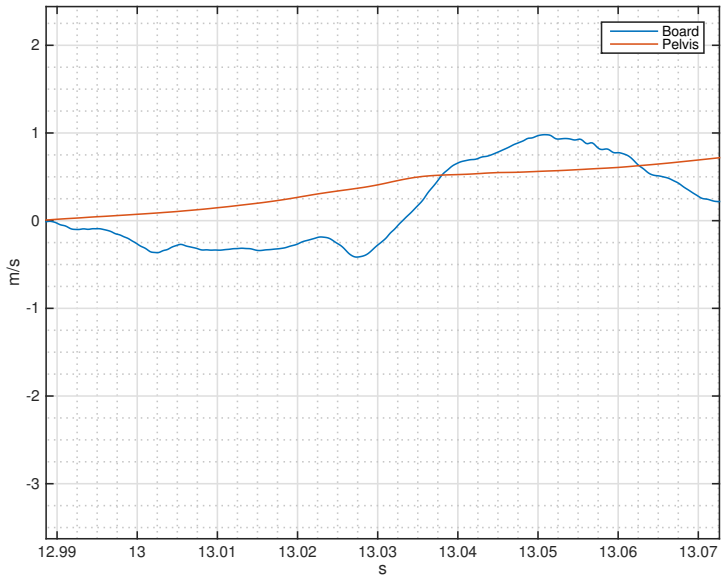


(b) Velocity

### A.3.7 7 trial

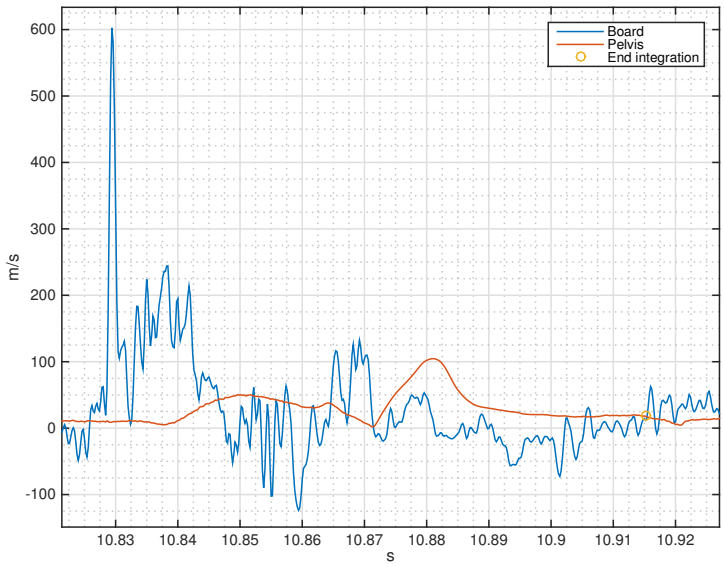


(a) Acceleration

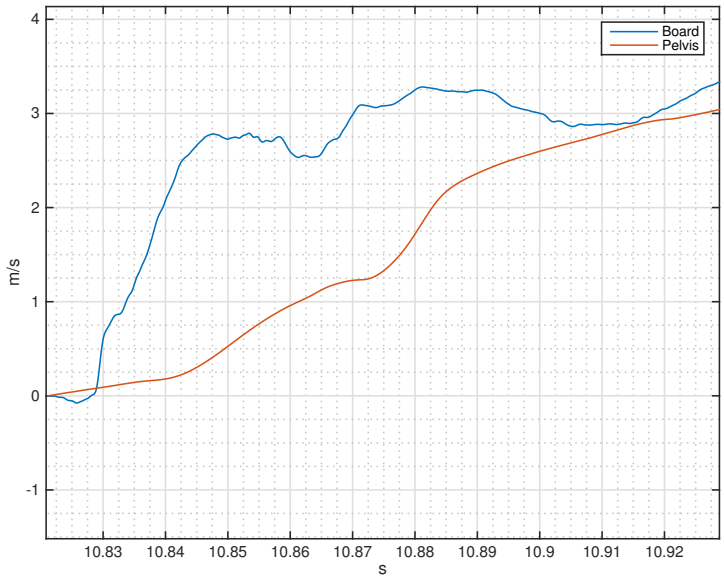


(b) Velocity

### A.3.8 8 trial

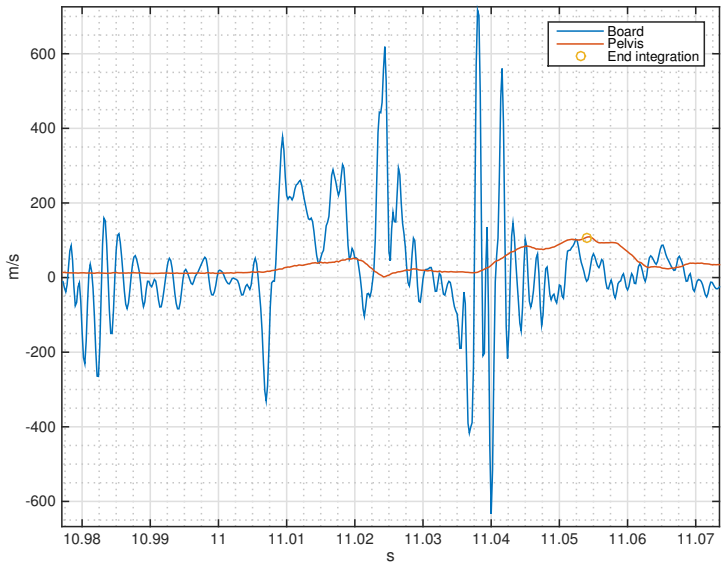


(a) Acceleration

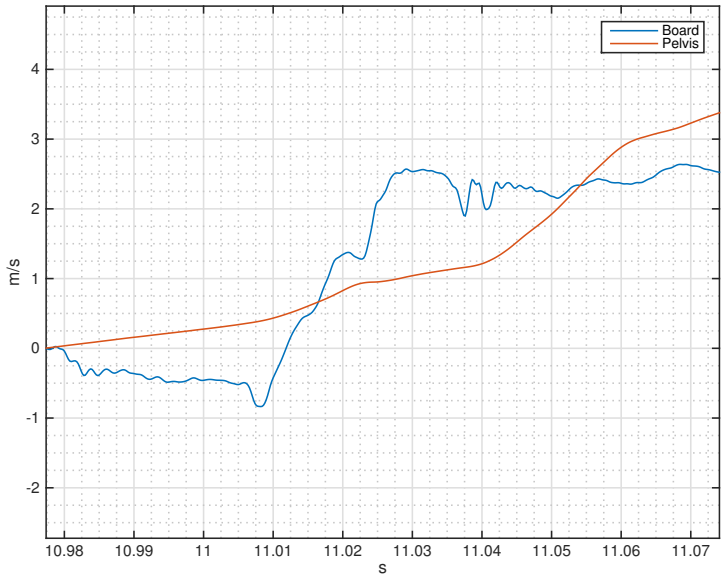


(b) Velocity

# References

[1] Mont Hubbard, James A. McNeil, Nicola Petrone, and Matteo Cognolato. Impact performance of standard tabletop and constant equivalent fall height snow park jumps, 8th September 2014.

[2] James A. McNeil and James B. McNeil. Dynamical analysis of winter terrain park jumps. *International Sports Engineering Association*, 2009.

[3] Mont Hubbard and Andrew Swedberg. Modeling terrain park jumps: Linear tabletop geometry may not limit equivalent fall height. *Skiing Trauma and Safety (ASTM STP1553)*, 2012.

[4] Mont Levy, Dean Hubbard, James A. McNeil, and Andrew Swedberg. Design of safer terrain park jumps using a graphical user interface, 23rd December 2014.

[5] James A. McNeil, Mont Hubbard, and Andrew Swedberg. Designing tomorrow's snow park jump. *International Sports Engineering Association*, 31st January 2012.

[6] Mont Hubbard. Ski jump impact energy reduction through landing surface shape design, 9th March 2015. 21th ISSS Conference, San Vito di Cadore (BL).

[7] James A. McNeil. Defining and measuring jumps: Developing terminology and test methods for creating freestyle terrain jump performance standards. Freestyle Terrain Jump Features Task Group ASTM F27.65, 9th March 2015. 21th ISSS Conference, San Vito di Cadore (BL).

[8] Mont Hubbard, James A. McNeil, Nicola Petrone, and Matteo Cognolato. Comparison of two ski jump landing surfaces: Equivalent fall height, 2014.

[9] Mont Hubbard and Andrew Swedberg. Terrain park jump landing surface design is robust to 'uncontrollable' factors, 6th November 2011.

[10] Mont Hubbard. Terrain park jump landing surface design is robust to 'uncontrollable' factors. *Journal of ASTM International*, December 2008.

[11] James A. McNeil. The inverting effect of curvature in winter terrain park jump takeoffs, 10th March 2012.